ANALYSIS AND SIMULATION OF A PWM CONVERTER DESIGNED TO PERFORM HARMONIC COMPENSATION AND MAXIMUM POWER POINT TRACKING IN A GRID-CONNECTED SOLAR SYSTEM

A Thesis

by

ANDRE EURICO DE MORAIS

Submitted to the Office of Graduate and Professional Studies of
Texas A&M University
in partial fulfillment of the requirements for the degree of

MASTER OF SCIENCE

Chair of Committee,	Mehrdad (Mark) Ehsani
Committee Members,	Chanan Singh
	Jose Silva-Martinez
	David Staack
Head of Department,	Miroslav M. Begovic

August 2016

Major Subject: Electrical Engineering

ABSTRACT

Solar energy is arguably the most promising response to the challenge of generating power in a clean and renewable way. However, there are many technical challenges that must be overcome before this alternative becomes able to replace the non-renewable sources in use today. For instance, currently there is no way to efficiently store the energy generated by photovoltaic panels while the sunlight is shining, which is crucial if energy generated by PV panels is to be used during the night or in a cloudy day. While those problems remain unsolved, one of the best ways available for using solar energy is to couple PV panels with the electric grid in order to minimize the use of non-renewable sources for power generation. This thesis presents and discusses the use of a power electronics based converter designed to couple a PV panel to the power grid. The converter in this case is able to extract the maximum power possible from the panel regardless of the environment conditions and perform harmonic compensation at the same time.

The thesis will be structured as follows. First, the theoretical foundation for analysis and design of the aforementioned converter will be presented. Then, the converter will be modeled. Using the model, a control system will be designed to enforce the desired behavior. Last, the whole system will be simulated in Matlab/Simulink® and the results will be analyzed.

DEDICATION

To my mother and my father (in memoriam)

To my sister Magda (in memoriam)

To my other sisters and my brother

To my beloved Nathalia G. Lemos

ACKNOWLEDGEMENTS

I would like to express my gratitude to Dr. M. Ehsani for his support, guidance, and words of wisdom throughout the course of my graduate studies. I would like to thank all of my committee members for their assistance. I also would like to express my appreciation to the faculty and staff of the Electrical Engineering Department at Texas A&M University for their support. I want to thank the Brazilian government who sponsored my studies through the CNPq agency. I also want to thank all the lab members who have helped me in many different ways during the last two years, particularly Mr. Abdullah Almehizia, Mr. Hussein Al-Masri and Mr. Nima F. Ershad. Last but not least I would like to thank my family and my girlfriend Nathalia G. Lemos for their unconditional support and encouragement throughout my thesis work and my studies.

TABLE OF CONTENTS

Page

LIST OF FIGURES

LIST OF TABLES

TABLE Page

1. INTRODUCTION

1.1 The importance of renewable sources of energy

1.1.1 The growing energy demand

It is difficult to overestimate the importance of energy for humanity. Basically, all human activities rely on some process in which energy is converted from one form to another. The understanding and/or control of those processes is undoubtedly the greatest achievement of mankind, who since the discovery of fire makes use of that knowledge to have more comfort, be safer and improve its quality of life. In this 21st century it would not be an exaggeration to say that the existence of humanity as we know it depends enormously on a high availability of energy.

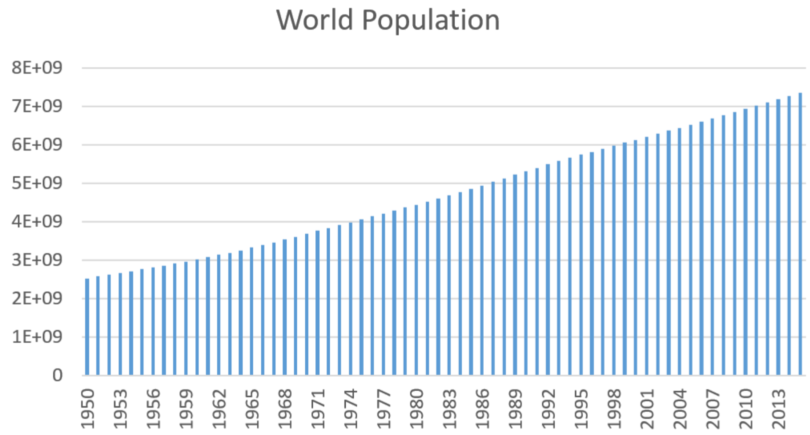

Figure 1.1: World population from 1950 to 2015.

There is more people living on Earth today than ever in history. In addition to that the energy consumption per capta has increased significantly over the past decades. Figure 1.1 shows that the world population has tripled in the last sixty five year, reaching the mark of 7,350,000,000 people in 2015. According to United

Nations estimation [18], that number will rise above 11,200,000,000 by 2100. The challenge of providing food and consumer goods for such a large population demands a significant increase in the current energy generation capacity. Figure 1.2 shows how the world energy demand has risen since the beginning of the 80s. In the reported period there was an increase of 85% in the energy consumption. Projections made by the U.S. Energy Information Administration estimate that by 2040 that number will be 56% higher than it was in 2010, reaching 232 trillion of kWh.

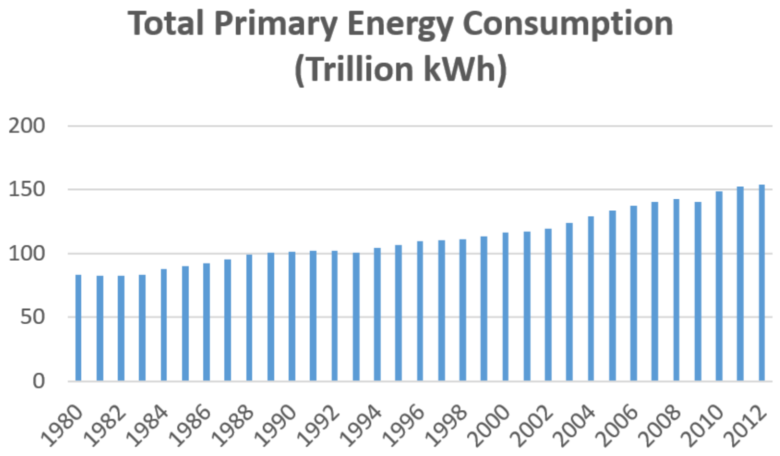

Figure 1.2: Total primary energy consumption from 1980 to 2012.

1.1.2 *Non-renewable sources depletion*

Fossil fuels stand for about 80% of all energy consumed in the world today[1]. According to U.S. Energy Information Administration predictions, by 2040 this percentage will still be as high as 78%[1]. However, there is no doubt that at the current consumption rate the non-renewable sources will be extinguished by some time in the future. Determining when this will happen is difficult since many different variables influence the process of exhaustion.

So far there is no consensus on how long the non-renewable sources will last. However, the majority of researches agree that it will not last much longer than a century [21]. That increases the necessity to transition from a fossil fuel based energy matrix to a renewable one.

1.1.3 Environmental problems

Another important aspect to be taken into consideration is the climate changes observed in the past few decades. Although man's role in that process still rises some controversy in non-specialized media, Cook et al [8] shows that the vast majority of climate experts consider anthropogenic activities the main cause of global warming. The most significant of those activities is the combustion of fossil fuels in vehicles, industrial parks and power plants. The burning process emits a large amount of carbon dioxide (besides other pollutant gases) which is a greenhouse gas.

The foreseen consequences of a continuous increase in the earth average temperature is catastrophic [19]. Because of that, international agreements aiming a significant reduction in the greenhouse gases emissions have been negotiated since the beginning of the 90s. That reduction can only be achieved if the use of fossil fuels is drastically reduced, which makes the task of meeting the world demand of energy even more challenging. In short, engineers not only will have to generate more energy in order to attend the needs of an increasing population, but will have to do so restricting the sources of energy to the clean ones.

1.2 Renewable sources of energy

The continuous increase in energy demand around the world, the expected exhaustion of fossil fuels within the next century and the high concern about global climate change has made renewable energy one of the most important topics for engineers today. Renewable sources are seen as the long-term solution for all the challenges enumerated above. They can provide as much energy as necessary, do not emit greenhouse gases and practically do not pollute the natural environment.

Accords like the Paris Agreement, sealed in 2015 during the 21st United Nations Conference of the Parties (COP21), indicate that the transition from non-renewable energy generation to renewable energy generation is gaining momentum. China, for instance, which is the greatest polluter in the world, has become the greatest investor in clean forms of energy. In 2014 the country invested US$ 83.3 billion in that field, 39% more than in 2013 and a world record. Germany, the sixth greatest consumer of energy in the world, is making massive investments to replace its nuclear plants by renewable sources. The European country is already extracting 27% of its energy from clean sources and has set the ambitious goal to rise that number to at least 80% by 2050. The United States, the world-leading producer of renewable energy in absolute terms and the second greatest investor in the sector, spent US$ 38.3 billion in 2014 and has recently established a world record of wind power generation.

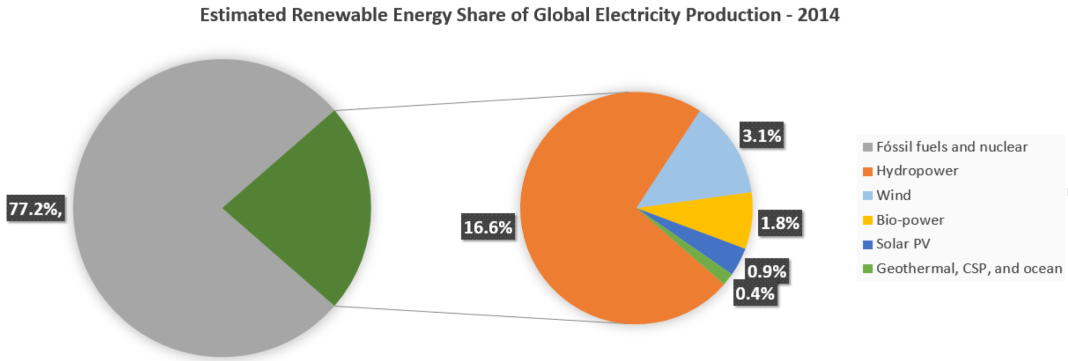

Figure 1.3: Estimated renewable energy share of global electricity production in 2014[10].

Figure 1.3 shows the estimated renewable energy share of global electricity production in 2014[7]. Renewable sources of energy contribute with almost 23% of the global electricity production. For the reasons mentioned before, that percentage is expected to increase steadily in the next decades.

Hydro power generation is currently the most important renewable resource, standing for about 65% of all clean energy generated in the world. However, it presents at least two important disadvantages when compared to other forms of green energy. First, not all the countries have water resources enough to construct the large dams usually required to generate electricity. Second, its generation model is intrinsically centralized.

Among the many different types of renewable sources, solar energy is seen as a very promising ones[12]. The energy that hits the Earth's surface in one hour coming from the Sun is more than the whole world needs in one year. With such an abundance, solar energy is an obvious alternative to replace the non-renewable sources in use today. However, there are great technological challenges to be overcome before that transition can happen. The most significant one is the lack of an efficient way to store electrical energy. That is important since the sun does not shine all day long. Another one is to reduce the costs of PV panels. Currently the price of solar generated electricity is still not attractive when compared to the electricity generated through fossil fuels[4].

There are two ways to use solar energy energy to generate electricity. The first one is to use a parabolic collector that concentrates all received light into a narrow region near its focus. By aligning a pipe with the focus of several collectors, a liquid flowing through the pipe can be heated up to the point that it evaporates. The generated steam can then be used to drive a electric power generator.

The second way is to use a photovoltaic panel (PV panel), a device made out of semiconductor material capable of directly converting solar energy into electricity.

This is the type of electricity generator that is considered in this thesis.

PV panels can be used in two different configurations that are discussed next.

1.3 Stand-alone PV system

The main characteristic of a stand-alone PV system is that it works independently of the electric grid. Figure 1.4 shows the main components of this configuration. The PV array is an interconnection of modules that provide the required photo-generated power to the system. The power rating of the PV array is determined based on the load requirements.

The battery bank is the element that allows the system to work when there is no sunlight. On a normal day, when the Sun is shining, the PV array converts the income irradiance into photo-generated power. The battery is constantly charged or discharged through the charge controller, depending on the balance between the power generated by the array and the load demand. The DC-AC converter converts the DC power to AC to supply the AC load. DC load is supplied form the DC link, before the DC-AC conversion.

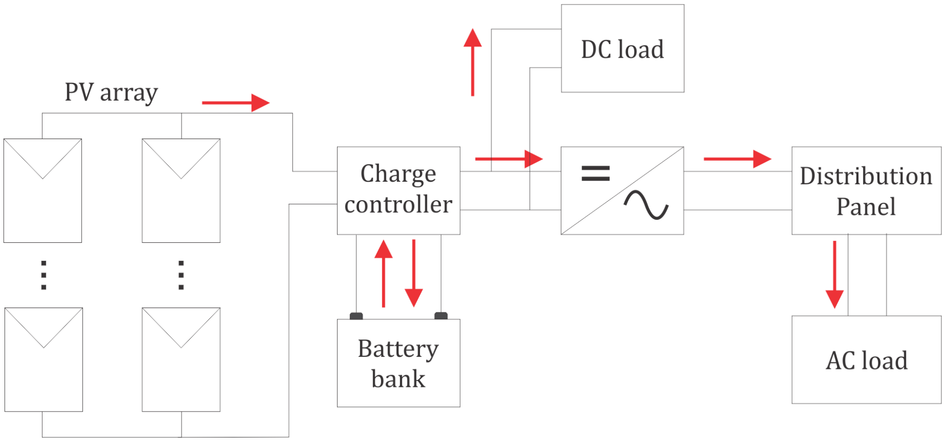

Figure 1.4: Stand-alone PV system components.

The system is designed in such a way that during a sunny day enough energy is generated to cover the load requirements at least during one night. However, in some situations the dark period can last longer than 12 hours, for instance, during rainy periods. In that case, the only way to continuously meet the load demand is to oversize the battery bank such that it gets more days of autonomy.

The problem with stand-alone system is the high cost associated especially with the battery bank. This configuration is recommended only in when remote installations that cannot access the electric grid must be powered.

1.4 Grid-connected PV system

Contrary to the stand-alone PV configuration, the grid-connected PV system operates connected to the electric grid. Figure 1.5 shows the main components of the system. In this configuration there is a continuous exchange of power between the system and the electric grid. This power exchange is controlled by the DC-AC converter, which is the backbone of the grid-connected PV system.

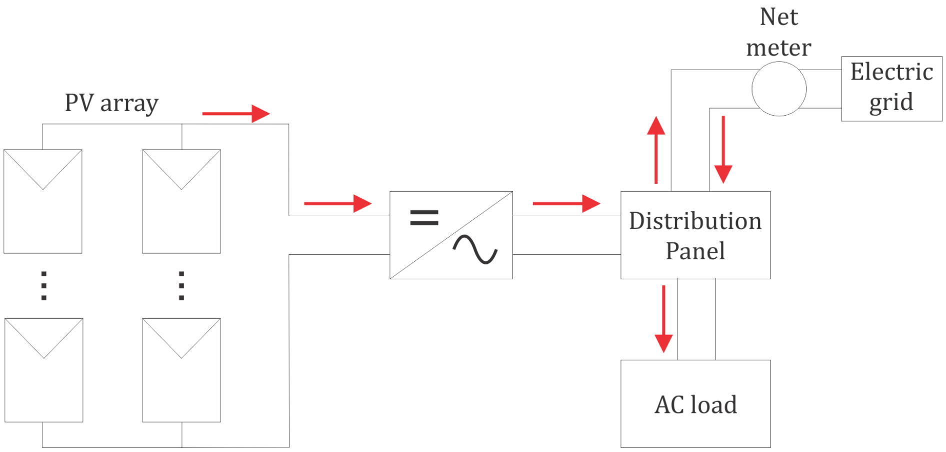

Figure 1.5: Grid-connected PV system components.

On a normal day, when the Sun is shining, the PV array converts the income irradiance into photo-generated power. The converter converts the DC power to AC to supply the AC load. Assuming that the power generated by the PV array is exactly the same as the load demand, no power is drawn from the electric grid.

On a very sunny day the PV array generates more power than the load needs. In that case, the net surplus power is directed to the electric grid. In some countries consumers are paid for the energy they feed to the grid. In order to account for that energy, a net meter must be installed between the system and the point of connection with the electric grid.

On a cloudy day the PV array provides less power than the load needs. In that situation the load demand is fulfilled by drawing the excess power from the grid, case in which the net meter will register a net consumption of power.

1.5 Motivation and objectives

The research project reported in this thesis is related to a grid-connected PV system. The goal is to use a the grid-connected converter described in the last section to extract the maximum power from the PV array and improve the quality of the system energy at the same time by doing harmonic compensation.

Harmonic compensation is required by regulatory agencies when the consumer load is non-linear. Without any compensation, that kind of load draws a highly distorted current from the electric grid, causing numerous problems to other consumers. Usually active filters are used to prevent that from happening. The goal of this research project is to make an active filter to extract the maximum power from a PV array under any environment condition, transmitting that power to the load and the grid when needed, while it executes its main task which is the harmonic compensation.

If that can be done, then money can be saved by making one converter to perform activities that otherwise would require two different converters.

1.6 Methodology

Due to time constraint the research project reported in this document was based on simulations only.

1.7 Thesis organization

The thesis will be organized as follows: chapter one introduces the problem and the context, giving also the motivation for the work. Chapter two will present the mathematical foundation used to analyze and model the converter. Chapter three presents the basics of photovoltaic technology. Chapter four shows the system modeling. Chapter five presents the design of the control system and some components of the power circuit. Chapter six presents the results got from simulation. Chapter seven gives a conclusion and suggestions for future work.

2. THE CLASSICAL AND INSTANTANEOUS POWER THEORIES

The classical definition of power, given in terms of voltage and current phasors, is valid only for systems operating under steady state conditions. Active, reactive and apparent power are calculated in terms of average values, which requires periodicity and is turns out to be inconvenient for determining power in a real time basis. For the system developed in this work a different definition of power, described in terms of instantaneous values, must be used. This chapter reviews the fundamental concepts of classical power theory and presents the Instantaneous Power Theory, an idea developed in the last few decades which is suitable for the application under investigation here.

2.1 The classical definition of power

The classical power theory was developed at the end of the 18th century with the advent of the AC electric systems. After a series of events that came to be known as *the battle of currents*, it became clear that AC power generation was the best alternative for long distance transmission of electricity. At that time, almost a century before the wide spread of modern electronic technology, the vast majority of loads were linear. Except for small transient periods, the whole system operated in sinusoidal regime, which made the classical power theory sufficient for analysis and design of electric systems.

The situation has changed considerably since the beginning of large scale production of electronic devices. Today the grid must supply power to a large amount of non-linear loads, which draw non-sinusoidal current even when supplied with sinusoidal voltage. The non-sinusoidal currents contain harmonics that may create voltage distortions in parts of the system, negatively affecting the distribution system and the load itself.

The following sub-sections will concisely present the most important concepts related to the classical power theory.

2.1.1 Definitions for single-phase circuits under sinusoidal regime

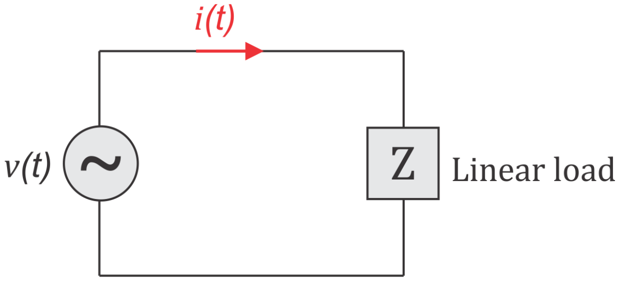

Figure 2.1: Single-phase circuit.

Figure 2.1 shows a schematic representation of a single-phase circuit comprised of a sinusoidal voltage source connected to a linear load. Since the load is linear, the current flowing through it is also sinusoidal. The source voltage $v(t)$ and the mesh current $i(t)$ can be described by

$$v(t) = V_p \cos(\omega t) \qquad i(t) = I_p \cos(\omega t - \phi) \tag{2.1}$$

where V_p and I_p are the peak values of $v(t)$ and $i(t)$ respectively. In circuit analysis it is usual to represent signals in terms of their root-mean-square(RMS) values. The RMS value of a periodic function $f(t)$ with period T is given by

$$F_{rms} = \sqrt{\frac{1}{T}\int_0^T f^2(t)dt} \tag{2.2}$$

Using the definition 2.2, it can be easily shown[17] that for a sinusoidal signal with peak value F_p, the correspondent RMS value is given by $F_p/\sqrt{2}$, which leads to a slightly different representation of $v(t)$ and $i(t)$:

$$v(t) = \sqrt{2}V_{rms}\cos(\omega t) \qquad\qquad i(t) = \sqrt{2}I_{rms}\cos(\omega t - \phi) \tag{2.3}$$

The voltage and current shown in equation 2.3 can be expressed as phasors, complex numbers that represent amplitude and phase of a sinusoidal signal. To illustrate this idea, observe that $i(t)$ in equation 2.3 can be seen as the real part of the complex number $\sqrt{2}I_{rms}e^{j(\omega t-\phi)}$, that is

$$\begin{aligned} i(t) &= \sqrt{2}I_{rms}\cos(\omega t - \phi) = Re\{\sqrt{2}I_{rms}e^{j(\omega t-\phi)}\} \\ &= Re\{\sqrt{2}I_{rms}e^{-j\phi}e^{j\omega t}\} = Re\{\bar{I}e^{j\omega t}\} \end{aligned} \tag{2.4}$$

Here, $\bar{I} = \sqrt{2}I_{rms}e^{-j\phi}$ is what is called the current phasor. Note that the phasor $\bar{I}$ bears information about the peak value and the phase shift of the current $i(t)$. Sometimes, instead of the peak value, the phasor amplitude is set to represent the RMS value of the sinusoidal signal. In that case the phasor is expressed as $\bar{I}_{rms} = I_{rms}e^{-j\phi}$. For the sake of compactness only amplitude and phase are represented in phasor notation. As an example, the current phasor shown in equation 2.4 is written as $\bar{I} = \sqrt{2}I_{rms}\angle-\phi$ or $\bar{I}_{rms} = I_{rms}\angle-\phi$. Figure 2.2 shows phasors $\bar{V}$ and $\bar{I}$ for three different types of load. The phasors rotate counterclockwise in the complex plane with a frequency ω and their projections on the real axis give the correspondent sinusoidal signals.

The instantaneous power flow between the voltage source and the load in the

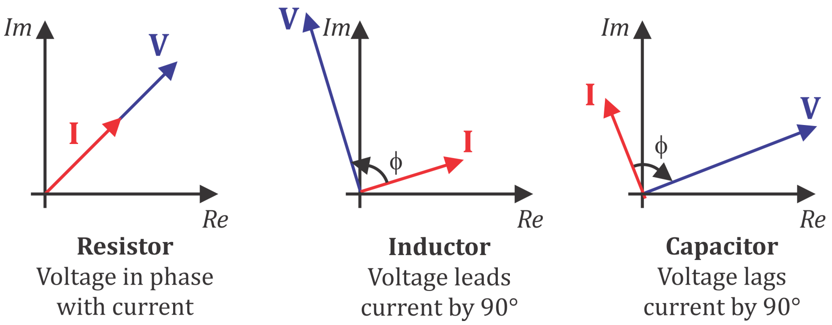

Figure 2.2: Phasor representation of voltage and current for three different types of impedance: resistive, capacitive and inductive

single-phase circuit shown in figure 2.1 is given by

$$\begin{aligned}p(t) &= v(t).i(t)\\ &= 2V_{rms}I_{rms}\sin(\omega t)\sin(\omega t+\phi)\\ &= V_{rms}I_{rms}\cos(\phi) - V_{rms}I_{rms}\cos(2\omega t-\phi)\\ &= V_{rms}I_{rms}\cos(\phi) - V_{rms}I_{rms}\cos(\phi)\cos(2\omega t) - V_{rms}I_{rms}\sin(\phi)\sin(2\omega t)\\ &= V_{rms}I_{rms}\cos(\phi)[1-\cos(2\omega t)] - V_{rms}I_{rms}\sin(\phi)\sin(2\omega t)\\ &= \underbrace{P[1-\cos(2\omega t)]}_{1^{\text{st}}\text{ part}} - \underbrace{Q\sin(2\omega t)}_{2^{\text{nd}}\text{ part}}\end{aligned} \tag{2.5}$$

where $P = V_{rms}I_{rms}\cos(\phi)$ and $Q = V_{rms}I_{rms}\sin(\phi)$. Equation 2.5 shows that $p(t)$ consists of two parts. The first one has an average value P and, superimposed on that, an AC component whose frequency of oscillation is twice the voltage source frequency. That part is always positive and represents the power flow from the source to the load. P represents the energy that actually drives the load, and for that reason it is conventionally called *active* power.

The second part has zero average. It represents a type of power that does not contribute to the net energy provided to the load. The energy transferred to the load during the first half cycle is returned back to the source in the second half cycle. The peak value of that part, Q, is what is called the *reactive* power. Although the reactive power has no effect in the net power transferred from the source to the load, it is highly undesirable to have it flowing forth and back in an electrical system. That is because it increases ohmic losses in transmission lines, making the whole system less efficient and causing a variety of other problems related to the overheat of transmission lines. Usually regulatory agencies limit to a minimum the amount of reactive power that a user can require from the power grid. The limits are typically given in terms of power factor, a concept that will shortly be discussed. Figure 2.3 shows a graphical representation of parts 1 and 2 of equation 2.5.

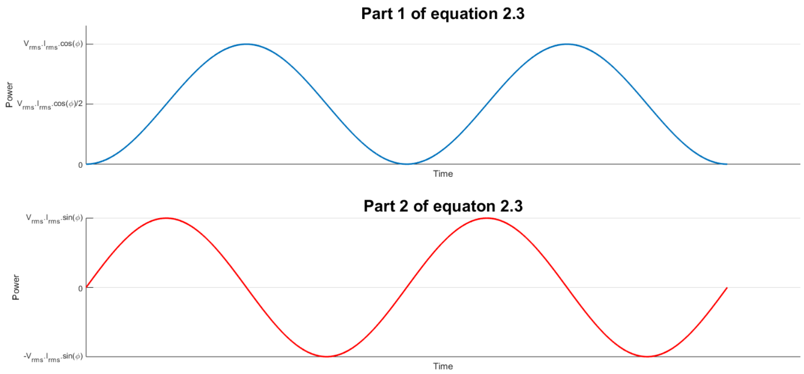

Figure 2.3: Part 1 and part 2 of equation 2.1.

Active and reactive powers can be represented as phasors in the complex domain, as shown in figure 2.4. The phasor $\bar{S}$ defines a new element, which is called the *complex* power. In mathematical terms, the complex power is given by

$$\bar{S} = \bar{V}_{rms}\bar{I}^{*}_{rms} = V_{rms}I_{rms}\angle\phi = V_{rms}I_{rms}(\cos\phi + j\sin\phi) = \bar{P} + j\bar{Q} \tag{2.6}$$

The magnitude of $\bar{S}$, given by $S = \sqrt{P^2 + Q^2} = V_{rms}I_{rms}$, is called the *apparent*

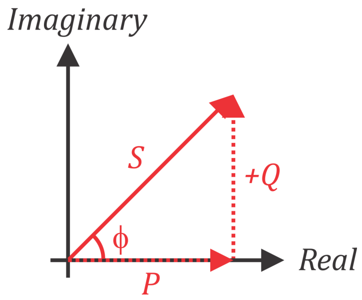

Figure 2.4: The power triangle.

power.

Another key concept in classical power theory is the power factor, which is defined as the ratio between active power and apparent power. For the sinusoidal steady-state condition considered in this section, the power factor is given by

$$PF = \frac{P}{S} = \frac{V_{rms} I_{rms} \cos(\phi)}{V_{rms} I_{rms}} = \cos(\phi) \tag{2.7}$$

Clearly, if $\phi = 0$, then $\cos(\phi) = 1$, $\sin(\phi) = 0$, $S = P$ and $Q = 0$. On the other hand, if $\phi = \frac{\pi}{2}$, then $\cos(\phi) = 0$, $\sin(\phi) = 1$, $Q = 0$ and $S = Q$. Thus, the power factor shows how the apparent power is distributed between active and reactive components. That is an indication of the system's efficiency: the greater the power factor, the more active power is produced, the less are the losses due to reactive power and the more efficient the system is. Ideally all the electric systems should operate with unit power factor. Utilities charge additional fees to customers who operate with a power factor below 90-95% for medium and large loads.

2.1.2 Definitions for single-phase circuits under non-sinusoidal regime

In the case of a system operating under non-sinusoidal conditions the previous formulas have to be modified. The periodic non-sinuoidal current and voltage can be decomposed into Fourier series as follows

$$\begin{aligned} v(t) &= V_0 + \sum_{n=1}^{+\infty} V_n \sin(n\omega_0 t + \phi_n) \\ i(t) &= I_0 + \sum_{n=1}^{+\infty} I_n \sin(n\omega_0 t + \phi_n) \end{aligned} \tag{2.8}$$

where V_0 and I_0 represent the average values of the source voltage and mesh current respectively. The Fourier coefficients V_n are calculated according to equation 2.9.

$$\begin{aligned} a_v &= \frac{2}{T}\int_{-T/2}^{T/2} v(t)\cos(n\omega_0 t)dt \\ b_v &= \frac{2}{T}\int_{-T/2}^{T/2} v(t)\sin(n\omega_0 t)dt \\ V_n &= \sqrt{a_v^2 + b_v^2} \end{aligned} \tag{2.9}$$

The coefficients I_n are calculated in an analogous way.

The average power is given by $\frac{1}{T}\int_0^T p(t)dt$. Equation 2.5 shows that the average of the voltage and current products at the same frequency is $V_{rms}I_{rms}\cos(\phi)$. The average of voltage and current products of different frequencies is zero. Thus, the average power in the non-sinusoidal regime is given by

$$P = V_0 I_0 + \sum_{n=1}^{\infty} V_{n,rms} I_{n,rms}\cos(\phi_n) \tag{2.10}$$

For the case in which a sinusoidal voltage source is applied to a non-linear load, only $i(t)$ will have harmonic components. In that case the average power will be given by

$$\begin{aligned} P &= (0)I_0 + V_{1,rms}I_{1,rms}\cos(\phi_1)\sum_{n=2}^{\infty}(0)I_{n,rms}\cos(\phi_n) \\ &= V_{1,rms}I_{1,rms}\cos(\phi_1) \end{aligned} \tag{2.11}$$

In that circumstance, a very common one in power systems, the power factor is calculated as shown in equation 2.12

$$PF = \frac{P}{S} = \frac{P}{V_{rms}I_{rms}} = \frac{V_{1,rms}I_{1,rms}\cos(\phi_1)}{V_{1,rms}I_{rms}} = \frac{I_{1,rms}}{I_{rms}}\cos(\phi_1) \tag{2.12}$$

The term $\frac{I_{1,rms}}{I_{rms}}$ in equation 2.12 is called the *distortion factor*(DF). It is worth noting that if the load is linear, $i(t)$ will have only the fundamental component, DF $= 1$ and the previous definition of power factor will be exactly the same as the one given in equation 2.7.

The *total harmonic distortion* is another figure of merit used to quantify the distortion in a system. It is defined as shown in equation 2.13

$$THD = \sqrt{\frac{\sum_{n\neq 1} I_{n,rms}^2}{I_{1,rms}^2}} = \sqrt{\frac{I_{rms}^2 - I_{1,rms}^2}{I_{1,rms}^2}} = \frac{\sqrt{\sum_{n=2}^{\infty} I_{n,rms}^2}}{I_{1,rms}} \tag{2.13}$$

Based on this definition, the distortion factor and the power factor can be rewritten as follows

$$DF = \frac{1}{\sqrt{1+THD^2}} \tag{2.14}$$

$$PF = \frac{1}{\sqrt{1+THD^2}}\cos(\phi) \tag{2.15}$$

2.1.3 Definitions for three-phase circuits

Generation, transmission and distribution of electrical power is commonly done using a particular type of system in which three voltage (current) sources are connected to each other in a symmetrical way. Usually, there is also some sort of symmetry between the voltage (current) amplitudes and phases of each source. This type of system is called a *three-phase* system.

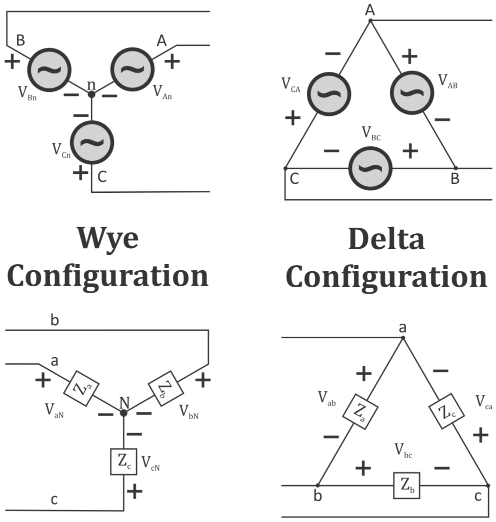

Figure 2.5: Three-phase voltage source and three-phase load configurations.

Three-phase systems are also comprised of three-phase loads. The sources as well as the loads can be set in two different configurations: wye and delta, as shown in figure 2.5. It follows that a three-phase systems comprising a three-phase voltage source and a three-phase load can be arranged in four different ways: wye-wye, wye-delta, delta-wye and delta-delta. For the purposes of this work it is enough do discuss only a few aspects of the wye-wye configuration.

Figure 2.6 shows the circuit representation of the aforementioned system. "n" is the common point of connection between the three single-phase voltage sources $v_{an}(t)$, $v_{bn}(t)$ and $v_{cn}(t)$. $i_a(t)$, $i_b(t)$ and $i_c(t)$ represent the currents flowing from the source to the load. The instantaneous three-phase power flow is given by

$$p(t) = v_{an}(t)i_a(t) + v_{bn}(t)i_b(t) + v_{cn}(t)i_c(t) \tag{2.16}$$

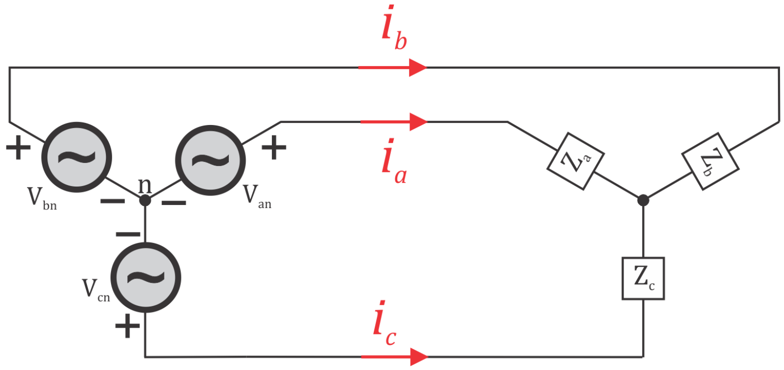

Figure 2.6: Three-phase system connected in a wye-wye configuration.

Ideally the three-phase system is balanced, that is, the phase voltages are sine waves with the same amplitude and phase shifted by 120° from each other, and each phase impedance has the same value. Equation 2.17 shows the mathematical representation of the phase voltages.

$$\begin{aligned} V_{an} &= V_{ph}\cos(\omega t) = V\angle 0^\circ \\ V_{bn} &= V_{ph}\cos(\omega t - 120^\circ) = V\angle - 120^\circ \\ V_{cn} &= V_{ph}\cos(\omega t + 120^\circ) = V\angle 120^\circ \end{aligned} \tag{2.17}$$

If the load connected to the voltage source is linear, the currents are also sinusoidal and can be represented by

$$\begin{aligned} i_a &= I_{ph}\cos(\omega t - \phi) = I_{ph}\angle - \phi \\ i_b &= I_{ph}\cos(\omega t - 120^\circ - \phi) = V\angle(-120^\circ - \phi) \\ i_c &= I_{ph}\cos(\omega t + 120^\circ - \phi) = V\angle(120^\circ - \phi) \end{aligned} \tag{2.18}$$

where $I_{ph} = \frac{V_{ph}}{|Z|}$. In that case equation 2.16 becomes

$$\begin{aligned} p_{3ph}(t) =& I_{ph}V_{ph}[\cos(\omega t)\cos(\omega t - \phi) + \cos(\omega t - 120^\circ)\cos(\omega t - 120^\circ - \phi) + \\ & \cos(\omega t + 120^\circ)\cos(\omega t + 120^\circ - \phi)] \\ =& \frac{3}{2} I_{ph}V_{ph}\cos\phi = 3I_{ph_{rms}}V_{ph_{rms}}\cos\phi = 3P \end{aligned} \tag{2.19}$$

Equation 2.19 shows that the instantaneous power flow in a three-phase balanced system with linear load is constant and equals 3 times the active power previously derived for a single-phase circuit (equation 2.5). This result provides an easy way to deal with balanced three-phase systems. Instead of working with all the voltages and currents simultaneously, an equivalent single-phase representation is derived from the original circuit and from that, the three-phase currents, voltages and power can be easily determined.

If the load is not linear, the current will be non-sinusoidal. In that case the definitions of THD, distortion factor and power factor, as defined in section 2.1.2, must also be applied.

It is clear from equation 2.2 that all the definitions given above rely on the knowledge of voltage and current values over an entire period. Thus, those definitions are not suitable for characterizing an electric system in a real time basis, when all the important physical quantities must be determined at each instant of time, neither it can be applied during transient regime, when no period is defined. The next section introduces a different set of definitions comprising the so called *instantaneous power theory*, which overcomes the aforementioned problems with the classical power theory.

2.2 The instantaneous power theory

2.2.1 Basic definitions

2.2.1.1 The dq0 Transformation

The instantaneous power theory, also called the "p-q theory", was first introduced by Akagi, Kanazawa and Nabae[2] in 1983. Differently from the conventional theory, the p-q theory is based on instantaneous values of voltage and current and is exclusively defined for three-phase systems. Originally it was defined in terms of the Clarke components of voltage and current. Here, an equivalent definition in terms of dq0 components of $v(t)$ and $i(t)$ will be presented. The dq0 transformation converts a three dimensional vector $\vec{F} = \begin{pmatrix} f_a & f_b & f_c \end{pmatrix}^T$ from a stationary coordinate frame (abc) to an orthogonal rotating frame (dq0). The transformation is defined as shown in equation 2.20

$$\begin{pmatrix} f_d \\ f_q \\ f_0 \end{pmatrix} = \sqrt{\frac{2}{3}} \begin{pmatrix} \cos(\omega_r t) & \cos(\omega_r t - \frac{2\pi}{3}) & \cos(\omega_r t + \frac{2\pi}{3}) \\ -\sin(\omega_r t) & -\sin(\omega_r t - \frac{2\pi}{3}) & -sin(\omega_r t + \frac{2\pi}{3}) \\ \frac{1}{\sqrt{2}} & \frac{1}{\sqrt{2}} & \frac{1}{\sqrt{2}} \end{pmatrix} \begin{pmatrix} f_a \\ f_b \\ f_c \end{pmatrix} \tag{2.20}$$

$$\vec{F}_{dq0} = P\vec{F}_{abc}$$

where $\omega_r t$ is the angular speed of the rotating reference frame. Here it will be assumed that the reference frame rotates with the same angular speed of $v(t)$ and $i(t)$, that is, $\omega_r = \omega$. P is the abc → dq0 transformation matrix. It is given by

$$P = \sqrt{\frac{2}{3}} \begin{pmatrix} \cos(\omega t) & \cos(\omega t - \frac{2\pi}{3}) & \cos(\omega t + \frac{2\pi}{3}) \\ -\sin(\omega t) & -\sin(\omega t - \frac{2\pi}{3}) & -sin(\omega t + \frac{2\pi}{3}) \\ \frac{1}{\sqrt{2}} & \frac{1}{\sqrt{2}} & \frac{1}{\sqrt{2}} \end{pmatrix} \tag{2.21}$$

The inverse dq0 transformation, that is, $\vec{F}_{dq0} \rightarrow \vec{F}_{abc}$, is shown in equation 2.22

$$\begin{pmatrix} f_a \\ f_b \\ f_c \end{pmatrix} = \sqrt{\frac{2}{3}} \begin{pmatrix} \cos(\omega t) & -\sin(\omega t) & \frac{1}{\sqrt{2}} \\ \cos(\omega t - \frac{2\pi}{3}) & -\sin(\omega t - \frac{2\pi}{3}) & \frac{1}{\sqrt{2}} \\ \cos(\omega t + \frac{2\pi}{3}) & -sin(\omega t + \frac{2\pi}{3}) & \frac{1}{\sqrt{2}} \end{pmatrix} \begin{pmatrix} f_d \\ f_q \\ f_0 \end{pmatrix} \tag{2.22}$$

$$\vec{F}_{abc} = P^{-1} \vec{F}_{dq0}$$

Evidently, given a set of three-phase voltage (or three-phase current), equation 2.20 can be used to perform the transformation $\vec{v}_{abc} \rightarrow \vec{v}_{dq0}$ ($\vec{i}_{abc} \rightarrow \vec{i}_{dq0}$).

2.2.1.2 Definitions of real, imaginary and zero-sequence power and its physical meaning

The p-q theory defines three power components in terms of the instantaneous values of voltage and current in the dq0 domain. Equation 2.23 presents the three definitions [3].

$$\begin{pmatrix} p_0(t) \\ p(t) \\ q(t) \end{pmatrix} = \begin{pmatrix} v_o(t) & 0 & 0 \\ 0 & v_d(t) & v_q(t) \\ 0 & v_q(t) & -v_d(t) \end{pmatrix} \begin{pmatrix} i_0(t) \\ i_d(t) \\ i_q(t) \end{pmatrix} \tag{2.23}$$

$p_0(t) = v_0(t) i_0(t)$ is the *instantaneous zero-sequence power.* $p(t) = v_d(t) i_d(t) + v_q(t) i_q(t)$ is called the *instantaneous real power* and $p(t) = v_q(t) i_d(t) - v_d(t) i_q(t)$ is the *instantaneous imaginary power.* Figure 2.7[3] helps to understand the physical meaning of the previous definitions. The instantaneous zero-sequence power + the instantaneous real power correspond to the instantaneous total power flow from the source to the load. The instantaneous imaginary power corresponds to the energy exchanged between the phases without transferring energy.

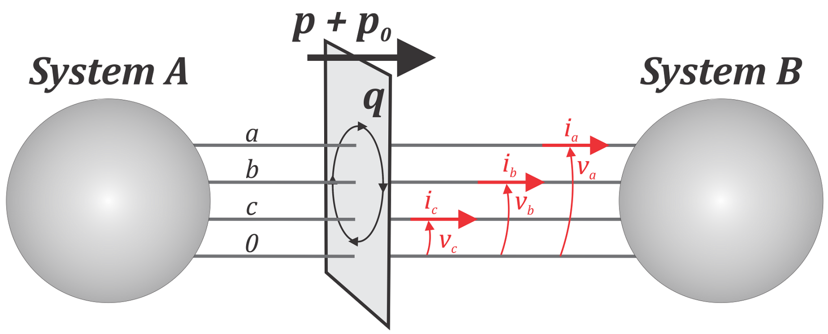

$p + p_0$: instantaneous total energy flow per time unit;
q: energy exchange between the phases without transferring energy.

Figure 2.7: Physical interpretation of p_0, p and q.[3]

$$\begin{pmatrix} f_d \\ f_q \end{pmatrix} = \sqrt{\frac{2}{3}} \begin{pmatrix} \cos(\omega_r t) & \cos(\omega_r t - \frac{2\pi}{3}) & \cos(\omega_r t + \frac{2\pi}{3}) \\ -\sin(\omega_r t) & -\sin(\omega_r t - \frac{2\pi}{3}) & -sin(\omega_r t + \frac{2\pi}{3}) \end{pmatrix} \begin{pmatrix} f_a \\ f_b \\ f_c \end{pmatrix}$$

$$\begin{pmatrix} f_a \\ f_b \\ f_c \end{pmatrix} = \sqrt{\frac{2}{3}} \begin{pmatrix} \cos(\omega t) & -\sin(\omega t) \\ \cos(\omega t - \frac{2\pi}{3}) & -\sin(\omega t - \frac{2\pi}{3}) \\ \cos(\omega t + \frac{2\pi}{3}) & -sin(\omega t + \frac{2\pi}{3}) \end{pmatrix} \begin{pmatrix} f_d \\ f_q \end{pmatrix} \tag{2.24}$$

$$\begin{pmatrix} p \\ q \end{pmatrix} = \begin{pmatrix} v_d & v_q \\ v_q & -v_d \end{pmatrix} \begin{pmatrix} i_d \\ i_q \end{pmatrix}$$

The three-phase system considered in this work is of the three-wire type. When a three-phase system does not have a neutral line, the zero-sequence current i_0 is zero, as well as the zero-sequence power p_0. Then, equations 2.20, 2.22 and 2.23 can be simplified as shown in equations 2.24. For that reason the zero components of power, voltage and current will be dismissed from this point on.

2.2.1.3 The relationship between classical power theory and instantaneous power theory

Each power defined above can be split into two different terms: a DC one, which corresponds to the average power, and an AC one, which has zero average and stands for the remaining Fourier components.

$$\begin{cases} p_0 = \overline{p_0} + \tilde{p_0} \\ p = \overline{p} + \tilde{p} \\ q = \overline{q} + \tilde{q} \end{cases} \tag{2.25}$$

There exists a relationship between the classical and the p-q theories of power. It can be shown[3] that the three-phase active power defined in the context of classical power theory is a subset of $\overline{p}$. In the same way, it can be shown that the three-phase reactive power defined before is a subset of $\overline{q}$. Thus, the classical theory of power is a particular case of the p-q theory, showing that the latter is more comprehensive than the former.

2.2.2 Using the p-q theory for harmonic compensation and power factor correction

One of the most important applications of the p-q theory is in the control of active power filters for harmonic compensation and power factor correction[3]. Figure 2.8 shows the typical situation in which power active filters are applied. A three-phase diode rectifier is connected between the grid (represented by the three-phase voltage source) and an inductive load. The rectifier controls the system power flow, ensuring that it goes from the AC side to the DC side. The rectifier draws a highly distorted current from the grid, frequently decreasing the power factor below the minimum value required by regulatory agencies, which makes necessary the use of some compensation technique. The compensation for the system illustrated in figure 2.8 is provided by the three-phase converter shown in the bottom part of the figure. The basic idea is to control the compensating current i_{Ca} such that it cancels the harmonic content present in the grid current i_{Sa}.

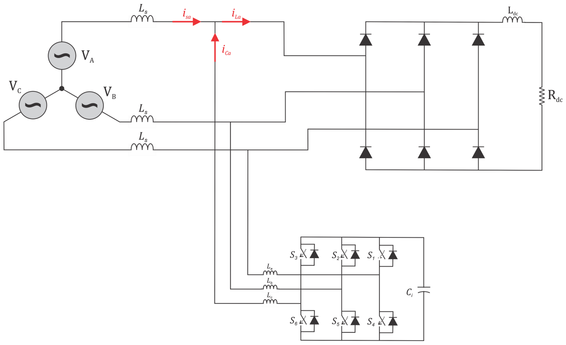

Figure 2.8: System configuration of a grid-connected shunt active filter.[3]

From the last equality in equation 2.24 it can be seen that

$$\begin{pmatrix} i_d \\ i_q \end{pmatrix} = \frac{1}{v_d^2 + v_q^2} \begin{pmatrix} v_d & v_q \\ v_q & -v_d \end{pmatrix} \begin{pmatrix} p \\ q \end{pmatrix} \tag{2.26}$$

From the previous discussion it is clear that the average energy per time unit transferred from the source to the load in a three-phase three-line system is given by the DC term of p in equation 2.25. The remaining terms, that is, the AC component of p and both components of q, are the ones related to the distortion and displacement of the current waveform. Those are the terms that the active filter must compensate for.

The procedure to perform the compensation is as follows. First, load current and voltage are measured and the resultant signal is converted to the dq0 domain. From v_d, v_q, i_d and i_q, p and q are determined according to equation 2.24. p is passed through a high-pass filter in order to separate $\overline{p}$ from $\tilde{p}$. Using $\tilde{p}$ and q, the compensation current are determined according to equation 2.26. The resulting signals i_{dc} and i_{qc} represent the currents that must be generated by the active compensator in order cancel out the distortion in the grid current. Those signals are used as reference in a control loop designed to perform PWM control of the compensator currents.

The voltage across the compensator capacitor is an important point to be considered. In order for the compensator to function properly, its capacitor needs to be charged. However, due to the power loss in the switches, the capacitor tends to discharge over time. The solution to this problem is to make the compensator to draw active power from the grid in order to balance the power loss in the switches. That can be done by adding an outer loop in the control system specially designed to control the voltage across the capacitor. Figure 2.9 shows a block diagram of the control scheme described above.

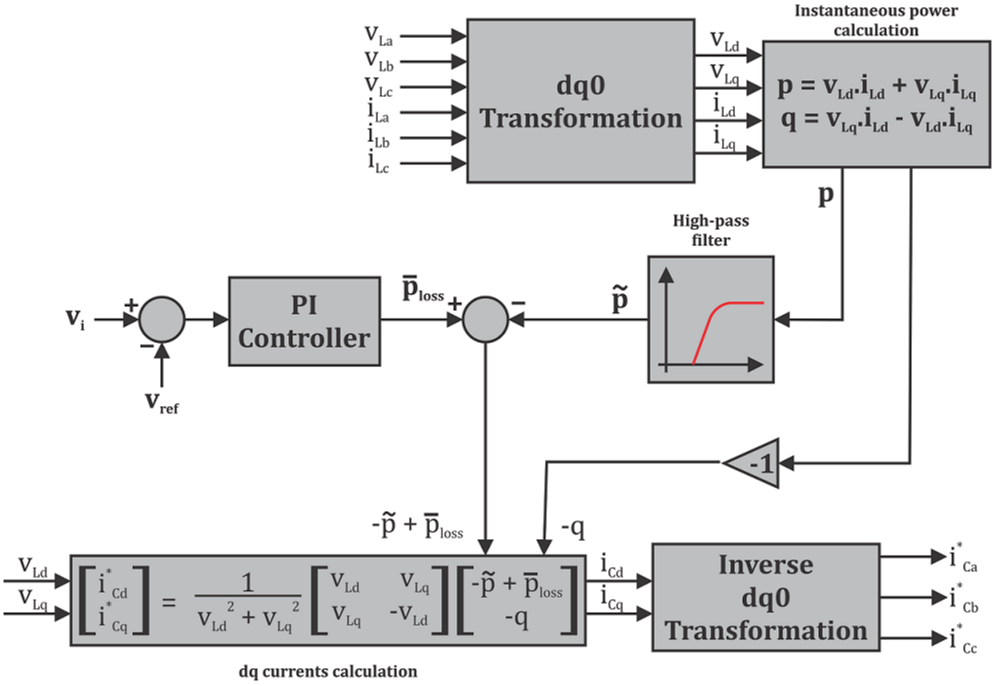

Figure 2.9: Block diagram of the control scheme.[3]

In chapter 5 the design of the control system will be shown in detail.

3. FUNDAMENTALS OF PHOTOVOLTAICS

Chapter 1 gave an overview of the role that photovoltaics can play in a renewable based power grid. It was discussed how solar energy is used in stand-alone and grid-connected applications. This chapter focuses on technical aspects of PV panels that are relevant to this work. Section 3.1 presents the physics of solar cells in a very concise way. The section's objective is to give a qualitative explanation about the solar cell features that will be explored later. The whole section is based on references [15] and [11]. Section 3.2 shows the terminal characteristics of PV panels based on the results given in section 3.1. Finally, section 3.3 discusses a few maximum power point tracking algorithms.

3.1 The physics of solar cells

A PV cell is basically a P-N junction that liberates carriers when exposed to light. When shaded, the cell behaves like a diode. When illuminated, photons interact with the semiconductor atoms originating an additional current.

The physics behind the solar cell can be understood on the basis of the electronic band theory of solids (EBT). The EBT explains the differences between conductors, semiconductors and insulators in terms of the possible energy states of an electron in a solid. Figure 3.1 helps to understand that difference. The valence band represents the highest energy states that electrons normally occupy when the solid is at zero absolute temperature, that is, at T = 0 K. Electrons in the valence band are bound to its respective atom and unable to take part in the electricity conduction process. The conduction band corresponds to the lowest vacant energy states that can be occupied by an electron. Electrons in the conduction band are not attached to any specific atom, they are free to move and therefore can conduct electricity. Between the two bands there is a range of energy states in which electrons cannot be, which is known as the band gap.

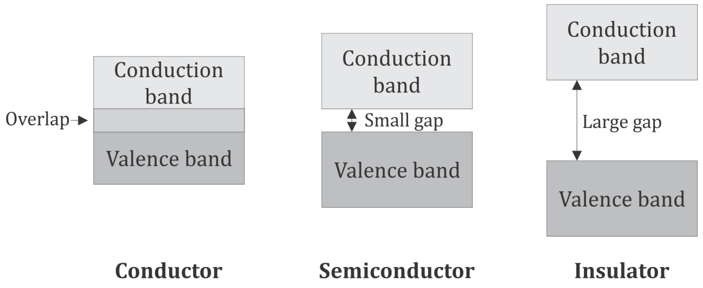

Figure 3.1: Conductors, semiconductors and insulators energy bands.

If electrons in the valence band are excited with an amount of energy higher than the band gap, they will change their energy state and will move to the conduction band. It is clear that the smaller the band gap, the easier it is for that process to happen. Figure 3.1 shows that the band gap of conductors is actually zero, that is, the conduction band overlaps the valence band. Thus, electrons in the valence band can easily reach the conduction band. In reality, at room temperature a conductor has billions and billions of electrons in its conduction band due to the thermal energy that it receives from the environment. That is what gives those materials the capability to conduct current. On the other hand, the band gap in insulators is large, making it difficult for electrons to transition from the valence band to the conduction band. Consequently, no electron is available to conduct electric energy in an insulator. Semiconductors fall in between conductors and insulators. It has a band gap that is not as small as the former neither large as the latter. It is such that electrons in the valence band need a relatively small amount of energy to jump into the conduction band. At room temperature a considerable number of electrons is already in the conduction band, although not enough to make the material a good conductor of electricity.

A way to excite the valence electrons of a semiconductor is to shine light on it. If the photons hitting the material have higher energy than the band gap, the electrons will absorb them and transition to the lowest vacant energy level in the conduction band. If the energy in the absorbed photons exceed the difference between the initial and the final states of energy, the difference will be converted into heat (see figure 3.2), which decreases the conversion efficiency. Since the main purpose of a solar cell is to convert energy from the sunlight into electricity, it is important to choose a semiconductor material whose band gap allows the maximum absorption of solar radiance with the highest efficiency possible.

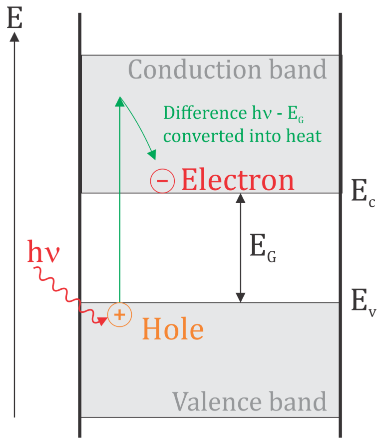

Figure 3.2: Illustration of the process of photon absorption by a semiconductor's electron.

Figure 3.3 shows the solar spectral irradiance. It can be seen that the maximum irradiance occurs around $\lambda = 550\ nm$. A photon with that wavelength has an energy equal to

$$E_{ph} = h\nu = h\frac{c}{\lambda} = 3.612 \times 10^{-19}\ J = 2.26\ eV \tag{3.1}$$

Thus, if the semiconductor has a bandgap of 2.26 eV, photons with $\lambda \leq 550\ nm$ will be absorbed by the material. On one hand, the vast majority of photons collected will have energy close to the material band gap, which means less heat and higher efficiency. On the other hand all the photons with $\lambda > 550\ nm$ will be missed and consequently a considerable amount of the available energy will not be harvested. Then, there is a trade off between efficiency and effective power conversion in the selection of the cell material.

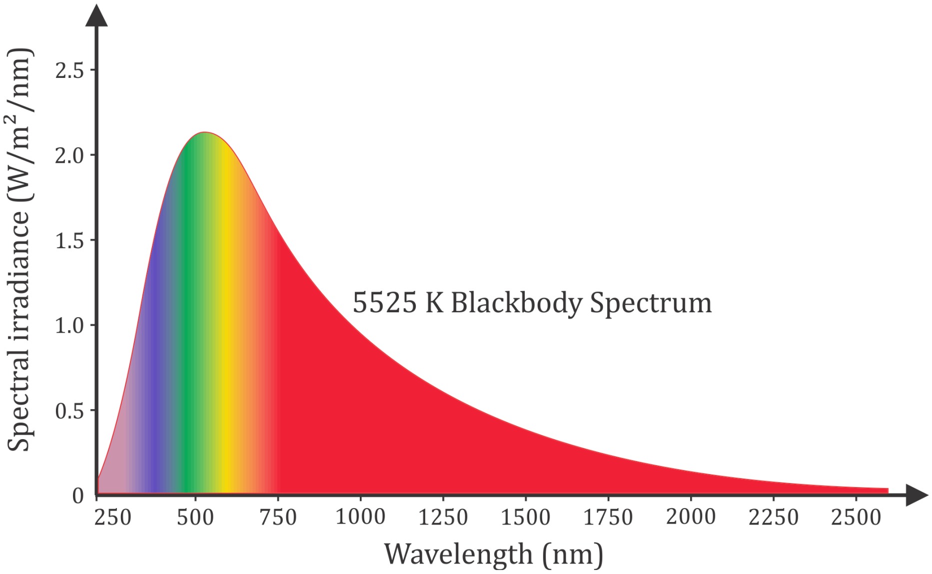

Figure 3.3: Sun irradiance spectrum

Usually, silicon(Si) is the material of choice. Using its band gap value given in table 3.1 it is easy to show that all the photons with $\lambda \leq 1118\ nm$ will be absorbed. From figure 3.3 it can be seen that more energy will be converted, however with a smaller efficiency since more heat will be generated.

In order to improve silicon conductivity, impurities are inserted into the silicon wafer in a process known as doping. In simple terms, the doping process consists

Table 3.1: Band gap energy for different semiconductors at 302 K.[13]

Material	E_g(eV)
InSb	0.17
InAs	0.36
Ge	0.66
GaSb	0.68
Si	1.11
InP	1.27
GaAs	1.43
CdTe	1.44
CdSe	1.74
GaP	2.25
ZnO	3.2
ZnS	3.6

in replacing silicon atoms, which have four valence electrons, by elements that have three and five. Normally boron and phosphorus are the elements used as dopants.

Intrinsic silicon is arranged in a regular lattice in which every atom forms a covalent bond with four other atoms surrounding it (see figure 3.4.a). When a silicon atom is replaced by a phosphorus atom, one of the five electrons in the phosphorus atom does not bond with the electrons of the neighbor atoms(see figure 3.4.b). Consequently, the electron can liberate itself from its nucleus and become available for electricity conduction. That kind of element contributes with an electron to the silicon lattice and is then called a “donor”. The resulting doped silicon is known as n-type silicon.

If the piece of silicon is doped with boron, only three electrons from the boron atom will bond with the three nearest silicon neighbors (see figure 3.4.c). The missing bond appears as a “hole”, which can be released into the substratum to take part in the electricity conduction. That kind of element contributes with a hole to the silicon lattice and is called an “acceptor”. The resulting doped silicon is known as

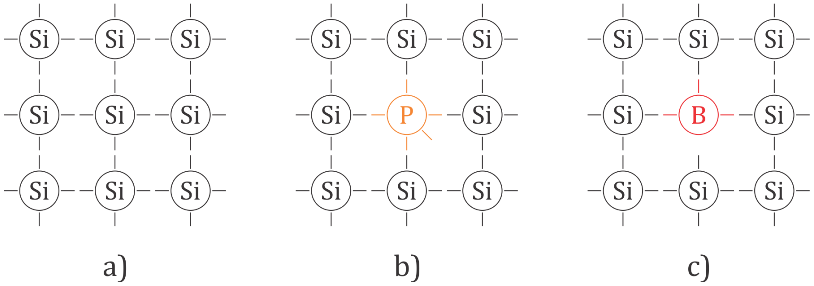

Figure 3.4: a) Intrinsic silicon, b) n-type silicon and c) p-type silicon

p-type silicon.

When p-type and n-type silicons are put together they form what is called a P-N junction (see figure 3.5). At first, electrons start to diffuse from the n-side to the p-side canceling out holes close to the junction region and ionizing the corresponding atoms. At the same time, every electron that moves from the n-side to the p-side leaves a positive ion in the n-side. Thus, a layer of fixed negative charge is formed in the p-side of the junction while a layer of fixed positive charge is formed in the n-side of the junction. The region between these two layers is known as the depletion zone.

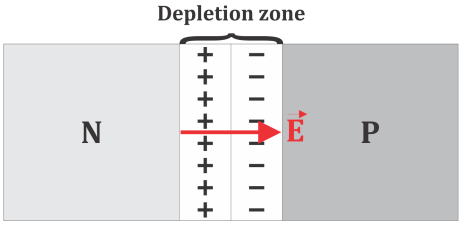

Figure 3.5: P-N junction

The fixed charges in the depletion zone originate an internal electric field, which in turn creates a drift of electrons from the p-side to the n-side. This electronic drift tends to decrease the length of the depletion zone, decreasing the electric field and consequently the drift current itself. Eventually the flux of electrons due to the drift equals the flux of electrons due to the diffusion and the length of the depletion zone becomes stable.

When shaded, this P-N junction behaves just like a diode. However, it changes when light shines on it. If a photon with higher energy than the silicon band gap hits the P-N junction, it makes an electron to move from the valence band to the conduction band creating an electron-hole pair (EHP). If the EHP is generated far from the junction, it will most likely to recombine and be lost. However, if the pair is generated in the depletion region it will be separated by the electric field present in that region with the electron going to the n-side and the hole going to the p-side. If an external connection is established between the n-side and the p-side of the P-N junction, the pair will circulate through the connection creating a current I_l. This photocurrent is directly proportional to the number of photons reaching the P-N junction, which is proportional to the irradiance level. If I_{l0} is the photocurrent at a known irradiance level G_0, then I_l can be calculated using equation 3.2, where G represents the irradiance at a given time and I_l the corresponding photocurrent.

$$I_l = \frac{I_0}{G_0} G \tag{3.2}$$

3.2 Terminal characteristics of PV cells

The solar cell described in section 3.1 can be ideally represented by the circuit shown in figure 3.6, where the current source represents the photocurrent discussed before and the diode stands for the P-N junction behavior when shaded. Mathematically, the cell can be described as in equation 3.3

$$I = I_l + I_0(e^{\frac{qV}{nkT}} - 1) \tag{3.3}$$

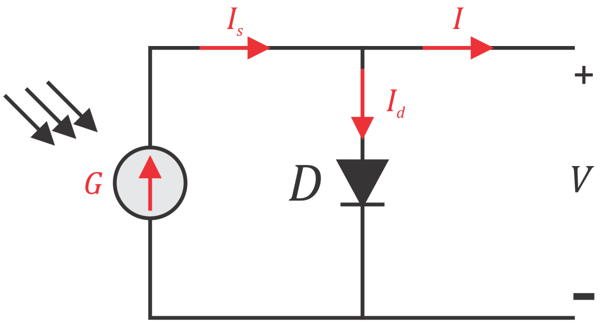

Figure 3.6: Ideal circuit model for the solar cell.

Here, I_l is photocurrent given by equation 3.2, I_0 is the diode saturation current, q is the electron charge ($= 1.6 \times 10^{-19} C$), V is the terminal voltage, n is the so called diode ideality factor, k is the Boltzmann's constant ($= 1.38 \times 10^{-23} \frac{m^2 kg}{s^2 K}$) and T is the junction absolute temperature.

Figure 3.7 shows the ideal solar cell I-V curve for four different irradiance levels. It can be seen that the cell has a limiting current and a limiting voltage and therefore can be safely operated under short-circuit or open-circuit condition. The figure shows that the irradiance strongly affects the short-circuit current while it has almost no effect on the open-circuit voltage. An expression for the short-circuit current can be found by setting V = 0 in equation 3.3.

$$I_{sc} = I_l + I_0(e^{\frac{q0}{nkT}} - 1) = I_l = \frac{I_0}{G_0} G \tag{3.4}$$

Equation 3.4 shows that, in the ideal case, the short-circuit current equals $\mathrm{I_l}$ which in turn is directly proportional to the irradiance G. Similarly, an expression for the open-circuit voltage is found by setting I = 0 in equation 3.3 and solving for V.

$$0 = I_l + I_0(e^{\frac{qV_{oc}}{nkT}} - 1) \Rightarrow V_{oc} = \frac{kT}{q} \ln(\frac{I_l + I_0}{I_0}) \cong \frac{kT}{q} \ln(\frac{I_l}{I_0}) \tag{3.5}$$

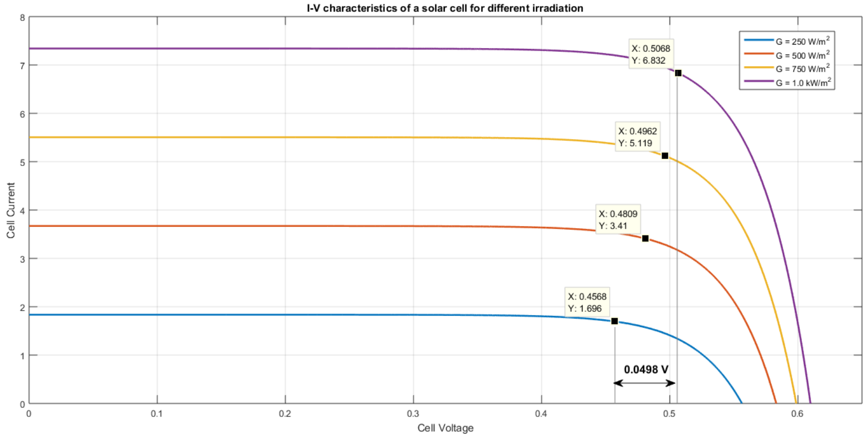

Figure 3.7: I-V characteristics of an ideal solar cell for different levels of illumination.

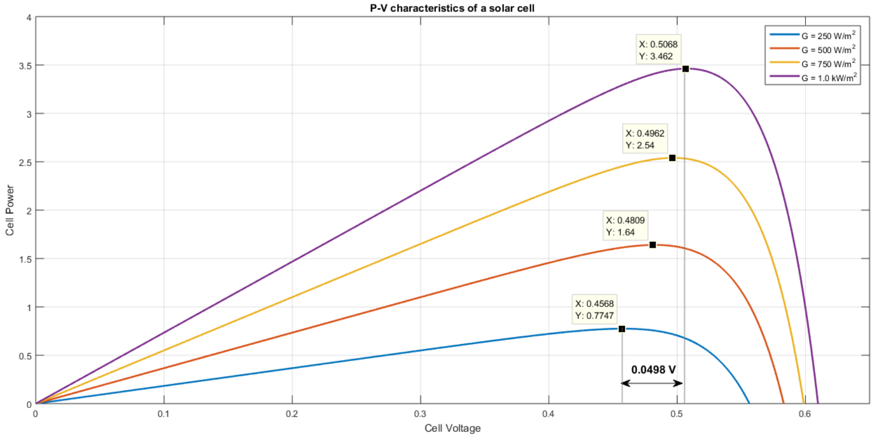

Figure 3.8: P-V characteristics of an ideal solar cell for different levels of illumination.

The cell output power can be calculated using the cell current and voltage. Figure 3.8 shows some P-V curves for different irradiances. The maximum power point of each curve is indicated by the black marker. It can be seen that although the maximum power changes considerably over that irradiance range, the voltage of the maximum power point does not. For a 75% change in the irradiance, the maximum power decreased 77% while maximum power voltage changed only 9.8%.

Equation 3.5 suggests that the open-circuit voltage is proportional to T. In reality,

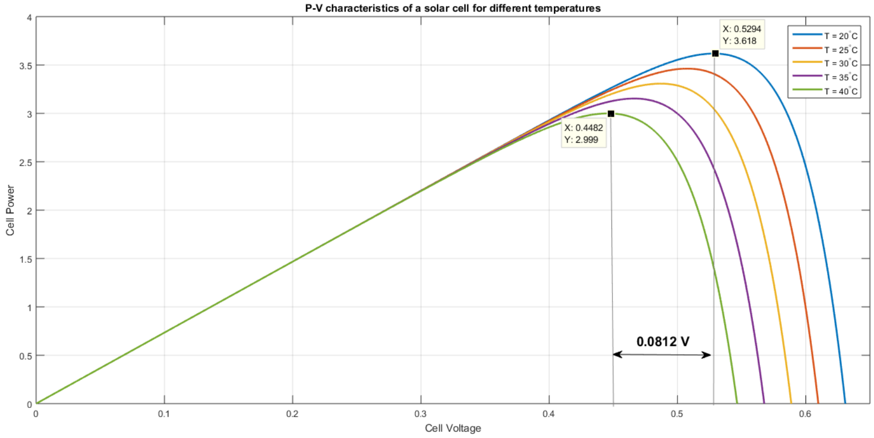

Figure 3.9: P-V characteristics of an ideal solar cell for different temperatures.

that is not the case. Actually I_0 has a strong dependence on the temperature, which makes the relationship between V_{oc} and T non-linear. It can be shown that V_{oc} decreases by 2.6 mV for every 1 °C increase in silicon cell temperature.

Figure 3.9 shows P-V curves for different temperatures. It makes clear that the maximum power decreases as the cell temperature goes up. It is worth noting that the maximum power voltage is more sensitive to temperature variation than to irradiance variation. For the case represented in figure 3.9, V_{mp} decreased 15% for a 20 °C increase in the cell temperature.

The open circuit voltage of single solar cells is around 0.65 V. In typical applications solar cells must be connected across points with rated voltage around a few hundred volts. If a single solar cell is used in that situation it will be damaged. In order to prevent that, solar cells are usually manufactured in modules, commonly known as PV panels. Each PV panel has a few strings of cells connected in parallel, each string having a few dozens of cells connected in series. Commercial PV panels typically have open-circuit voltages is in the order or 30 V. Those PV panels are combined in arrays in order meet the requirements of specific applications.

3.3 Maximum power point tracking algorithms

Figures 3.8 and 3.9 show that for every irradiance level and temperature there is a unique operational point in which the solar cell output power is maximum. In the vast majority of applications it is highly desirable to operate the PV panel near the maximum power point. By extracting the maximum power from a PV panel one reduces the number of panels necessary to meet the load power requirement, reducing then the system's implementation cost.

One of the challenges to the implementation of PV panels is to operate it at the maximum power point independently of the temperature and irradiance level. That is usually done with the help of a closed-loop system with a digital controller, which is able to implement algorithms to track the optimum operational point under any condition. This section presents three of the most popular maximum power point tracking (MPPT) algorithms.

In stand-alone applications the storage elements may be completely charged at some point and the power being converted by the panels still be greater than the load demand plus the losses. That imposes another challenge to the system, which is the power management. In that hypothetical situation the PV panels would have to be operated in a less than optimum point. In the application considered in this thesis that is not a problem. In the grid-connected PV system any power surplus can be directed to the grid, allowing the PV panels to operate at its optimum point all the time.

3.3.1 Constant voltage method

The constant voltage method is based on the observation that the voltage at maximum power point does not vary too much as the irradiance level changes. It was shown previously that V_{mp} varies around 10% when the incident irradiance changes from 1 kW/m^2 to 250 W/m^2(see figure 3.8). Thus, if the voltage across the PV panel is kept constant at an appropriate value, the power will not decrease too much as the irradiance changes. It was empirically observed that the voltage at the maximum power point is around 70%-80% of the V_{oc} at standard atmospheric conditions[9]. By measuring that value of V_{oc} one can easily determine a reasonable value for the voltage across the PV panel to be fixed at.

One advantage of this method is its simplicity. It requires only one measurement of V_{oc} and no closed-loop control system. On the other hand it does not track the maximum power point and lead to a less-than-optimum operation of the PV panel. It was previously shown that the maximum power point temperature is more sensitive to changes in the cell temperature than in irradiance level. Therefore, this method is recommended for places where the temperature does not change considerably.

3.3.2 Perturb and observe algorithm (P&O)

The perturb and observe algorithm is probably the most used one in practical applications. The method principles are very simple: the terminal voltage of the PV panel is periodically incremented or decremented while the output power is observed. If the power increases from one clock cycle to the other, the controller keeps changing the terminal voltage in the same way it did in the previous cycle. For example, if an increase in the terminal voltage results in an increase in the output power, the controller keeps increasing the terminal voltage. On the contrary, if the power decreases from one clock cycle to the other, the controller starts to change the terminal voltage in the opposite way. For instance, if an increase in the terminal voltage results in a decrease in the output power, the controller starts to decrease the terminal voltage. Figure 3.10 shows the flowchart of a possible implementation of the P&O algorithm.

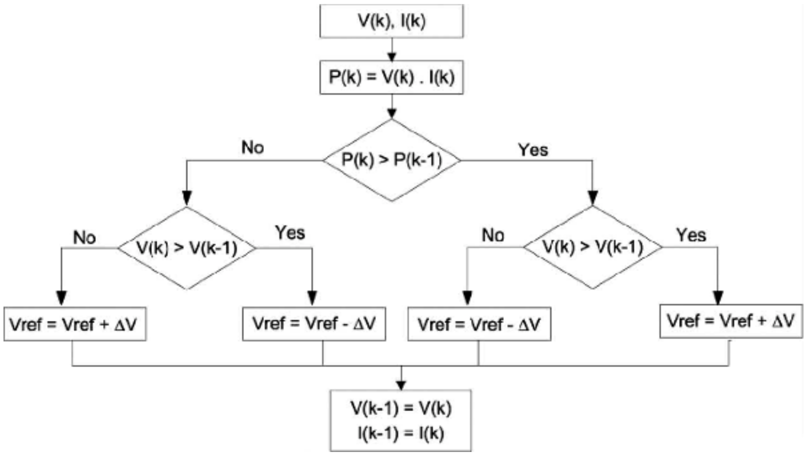

Figure 3.10: Flowchart of perturb and observe MPPT algorithm.

The parameter ΔV shown in the flowchart is the step size by which the panel terminal voltage is increased or decreased. It affects how fast the system tracks the optimum voltage and also the voltage fluctuation in the steady state. The bigger the step size, the faster V_{mp} is reached and the bigger the steady state voltage fluctuation is. The opposite also holds true. Figure 3.11 illustrates the effect of ΔV. From top to bottom, the step size has been increased in each simulation. The first simulation is the one with the smallest step size. It can be seen that the steady state voltage is reached in about 0.31 seconds, with a voltage ripple of about 7 V in the steady state. The second simulation shows that with a little larger step size, the system takes only 0.11 seconds to reach the steady state. However, once the voltage reaches the steady state the ripple is about 20 V. Finally, the last simulation shows that with the biggest step size the transient period is just 0.05 seconds, but the voltage ripple in the steady state is largest one, about 46 V.

It is possible modify the P&O algorithm in order to have an adaptive step size,

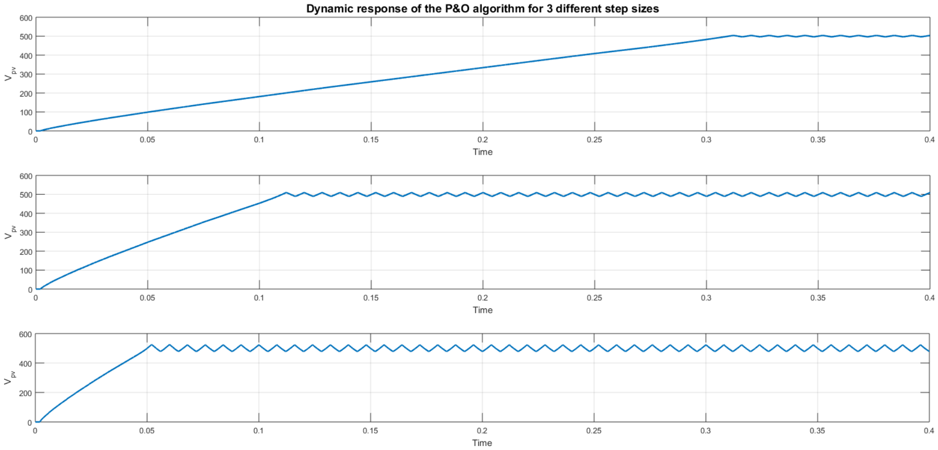

Figure 3.11: P&O algorithm response for three different values of V.

making it large at the beginning of the tracking process and small (tending to zero) as the terminal voltage reaches the steady state. That variation of the P&O algorithm will not be further discussed in this thesis.

3.3.3 Incremental conductance algorithm (IC)

The incremental conductance method is based on the relationship between the instantaneous conductance and the incremental conductance in a solar cell. Figure 3.12 helps to understand that relationship. The derivative of power versus voltage has different sign depending on whether the terminal voltage across the panel is smaller, greater or equal to the maximum power point voltage. At the maximum power point, $\frac{dP}{dV} = 0$. If the panel voltage is smaller than $\mathrm{V_{mp}}$, then $\frac{dP}{dV} > 0$; if it is greater, then $\frac{dP}{dV} < 0$. Since $P = VI$, $\frac{dP}{dV}$ at the MPP is given by

$$\frac{dP}{dV} = \frac{d(IV)}{dV} = \frac{dI}{dV}V + I = 0 \Rightarrow \frac{dI}{dV} = -\frac{I}{V} \tag{3.6}$$

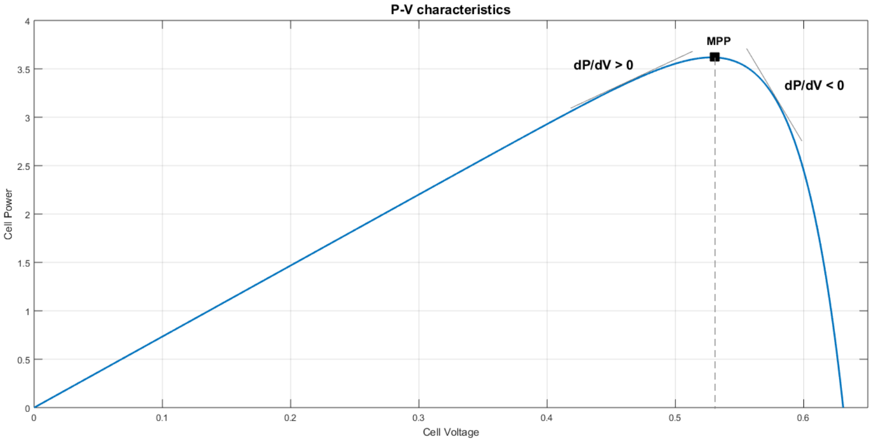

Figure 3.12: P-V characteristics of a solar cell

If ΔV is small, $\frac{dI}{dV}$ can be approximated by $\frac{\Delta I}{\Delta V}$ and the previous expression becomes $\frac{\Delta I}{\Delta V} = -\frac{I}{V}$. Thus, by comparing the incremental conductance $\frac{\Delta I}{\Delta V}$ to the instantaneous conductance $\frac{I}{V}$, the algorithm can determine in which region of the P-V curve the system is operating and how the terminal voltage should be changed in the next cycle. If $\frac{\Delta I}{\Delta V} = -\frac{I}{V}$, the system is exactly at the maximum power point and the terminal voltage should be kept constant. If $\frac{\Delta I}{\Delta V} > -\frac{I}{V}$, the system is operating in the left side of the MPP and the voltage should be increased. Finally, if $\frac{\Delta I}{\Delta V} < -\frac{I}{V}$, the system is operating in the right side of the MPP and the terminal voltage should be decreased.

Based on the algorithm description given in the last paragraph, the terminal voltage will be locked at $\mathrm{V_{mp}}$ once it gets there. However, if the illumination or temperature changes and the terminal voltage does not, the system will be operating in a less-than-optimum point. In order to prevent that from happening, the system monitors the output current in order to catch any change of power when the terminal voltage is being kept constant. If $\Delta V = \Delta I = 0$, the system is operating at the MPP and nothing must be done. If $\Delta V = 0$ and $\Delta I > 0$, that means the illumination

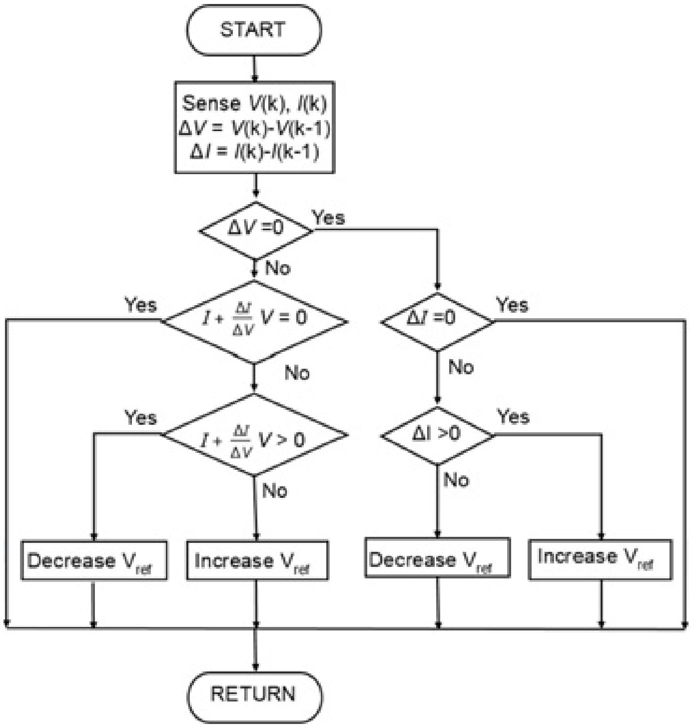

Figure 3.13: Flowchart describing the IC algorithm.

has increased or the temperature has decreased and in any of those situations the terminal voltage must be increased. If $\Delta V = 0$ and $\Delta I < 0$, illumination has decreased or temperature has increased and the terminal voltage must be decreased. Figure 3.13 shows a flowchart description of the incremental conductance algorithm.

As the P&O method, the IC algorithm must monitor the panel current and voltage. However, it does not need to calculate the output power, softening a little the computational requirements of the digital controller[9].

This chapter has presented the basic technical information about PV panels that will be used in the work. Next chapter will present the modeling of the converter that constitutes the core of the system discussed in this thesis.

4. THE PWM CONVERTER MODELING

In section 2.2.2 it was briefly discussed how active filters are used for harmonic compensation and power factor correction of three-phase loads. Section 3.3 explained how MPPT algorithms can ensure optimum operation of a PV panel by controlling the voltage across its terminals. This chapter utilizes those concepts to show how an active filter can be used to extract the maximum power from a grid-connected PV panel while doing harmonic compensation. The modeling presented here is based on references [5], [6], and [20].

4.1 The three-phase PWM converter

Figure 2.8 showed schematically a shunt active filter connected between a non-linear load and the power grid performing harmonic compensation. Here it will be show how a PV panel can be connected across the active filter capacitor in order to help the grid to supply power to the load while performing harmonic compensation and power factor correction.

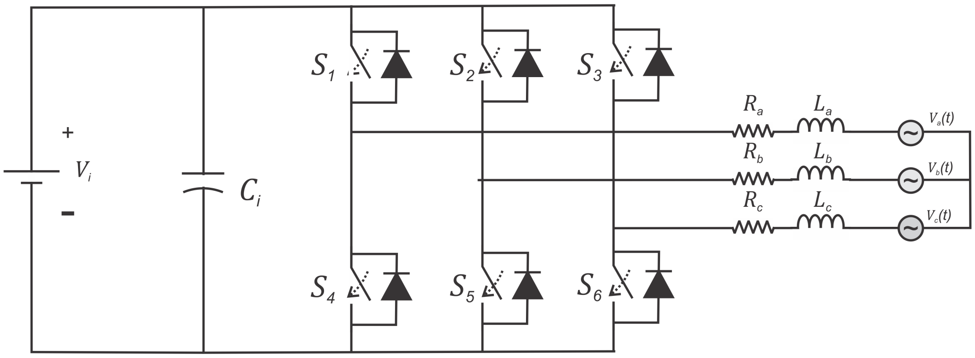

Figure 4.1: System considered in the development of the converter model.

The shunt active filter itself is just a bidirectional DC-AC three-phase converter with PWM modulation. What makes it so powerful in performing harmonic compensation is the control system coupled with it. In order to design an efficient control system, it is necessary to have a converter model.

The converter model will be developed in the dq0-domain based on the system illustrated in figure 4.1. It will be assumed that $V_a(t)$, $V_b(t)$ and $V_c(t)$ form a balanced set of voltages sources, which is a reasonable assumption since the voltage sources are modeling the grid voltages. The phase voltages can be described by

$$\begin{aligned} V_a &= V_{ph}\sin(\omega t) \\ V_b &= V_{ph}\sin(\omega t - 120^\circ) \\ V_c &= V_{ph}\sin(\omega t + 120^\circ) \end{aligned} \tag{4.1}$$

The line voltages are given by

$$\begin{aligned} V_{ab} &= V_a - V_b = \sqrt{3}V_{ph}\sin(\omega t + 30^\circ) \\ V_{bc} &= V_b - V_c = \sqrt{3}V_{ph}\sin(\omega t - 90^\circ) \\ V_{ca} &= V_c - V_a = \sqrt{3}V_{ph}\sin(\omega t + 150^\circ) \end{aligned} \tag{4.2}$$

In the modeling process this set of line voltages will be transformed into the dq0 domain. It is convenient to have the voltage V_{ab} in phase with the direct axis of the dq0 reference frame. In order to ensure that, the reference frame used in the last two set of equations must be delayed by 60°. Equation 4.2 can be then rewritten as

$$\begin{aligned} V_{ab} &= \sqrt{3}V_{ph}\sin(\omega t + 90^\circ) = \sqrt{3}V_{ph}\cos(\omega t) \\ V_{bc} &= \sqrt{3}V_{ph}\sin(\omega t - 30^\circ) = \sqrt{3}V_{ph}\cos(\omega t - 120^\circ) \\ V_{ca} &= \sqrt{3}V_{ph}\sin(\omega t + 210^\circ) = \sqrt{3}V_{ph}\cos(\omega t + 120^\circ) \end{aligned} \tag{4.3}$$

It will be assumed that V_i, the input voltage, is constant. In the actual system it is not, but it changes very slowly, such that it can be approximated by a constant voltage source.

The converter modeling will be done in two parts. First, a model for current control will be obtained. This first model will be used to design a controller for harmonic compensation purposes. Second, a model for input voltage will be developed. This second model will be useful to design a controller that implements MPPT algorithms to extract the maximum power from the PV array.

4.1.1 The model for current control

The converter shown in figure 4.1 can be represented without loss of generality by the simplified circuit shown in figure 4.2. Observing the figure, it can be seen that when switch $\mathrm{S_a}$ is in position $\mathrm{A_1}$, the voltage at the phase A switch will be $\mathrm{V_i}$ and when $\mathrm{S_a}$ is in position $\mathrm{A_0}$, the voltage of phase A will be 0. The same holds for switches $\mathrm{S_b}$ and $\mathrm{S_c}$. If $\mathrm{D_a}$, $\mathrm{D_b}$ and $\mathrm{D_c}$ are the duty cycles of the respective switches, the switches' voltage can be represented by

$$\begin{aligned} V_{Ca}(t) &= D_a(t)V_i \\ V_{Cb}(t) &= D_b(t)V_i \\ V_{Cc}(t) &= D_c(t)V_i \end{aligned} \tag{4.4}$$

The circuit in figure 4.2 can be redrawn as shown in figure 4.3. Applying Kirchhoff's voltage law to the three loops shown in the circuit of figure 4.3 the following equations are generated

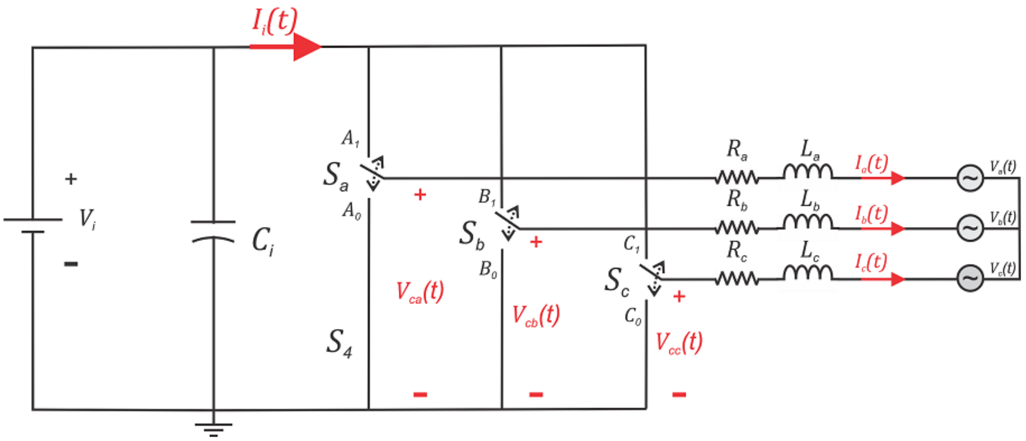

Figure 4.2: Equivalent model of circuit 4.1.

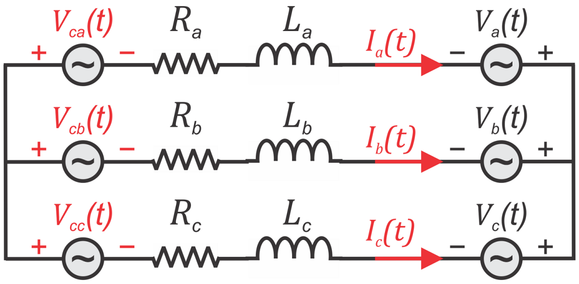

Figure 4.3: Equivalent model of circuit 4.2.

$$\begin{aligned}
V_a - V_b &= (V_{La} - V_{Lb}) + (V_{Ca} - V_{Cb}) + (V_{Ra} - V_{Rb}) \\
V_b - V_c &= (V_{Lb} - V_{Lc}) + (V_{Cb} - V_{Cc}) + (V_{Rb} - V_{Rc}) \\
V_c - V_a &= (V_{Lc} - V_{La}) + (V_{Cc} - V_{Ca}) + (V_{Rc} - V_{Ra})
\end{aligned} \tag{4.5}$$

$$\begin{aligned}
V_a - V_b &= (V_{La} - V_{Lb}) + (D_a - D_b)V_i + (V_{Ra} - V_{Rb}) \\
V_b - V_c &= (V_{Lb} - V_{Lc}) + (D_b - D_c)V_i + (V_{Rb} - V_{Rc}) \\
V_c - V_a &= (V_{Lc} - V_{La}) + (D_c - D_a)V_i + (V_{Rc} - V_{Ra})
\end{aligned} \tag{4.6}$$

If we assume that the system is balanced, $R_a = R_b = R_c = R$ and $L_a = L_b = L_c$

= L. The previous equation can then be compressed as follows

$$\begin{aligned} V_{ab} &= V_{Lab} + D_{ab}V_i + V_{Rab} \\ V_{bc} &= V_{Lbc} + D_{bc}V_i + V_{Rbc} \\ V_{ca} &= V_{Lca} + D_{ca}V_i + V_{Rca} \end{aligned} \tag{4.7}$$

The voltages across the inductor and resistors are given by

$$\begin{aligned} V_{Lab} &= L\frac{dI_{ab}}{dt} \\ V_{Lbc} &= L\frac{dI_{bc}}{dt} \\ V_{Lca} &= L\frac{dI_{ca}}{dt} \end{aligned} \tag{4.8}$$

and

$$\begin{aligned} V_{Rab} &= RI_{ab} \\ V_{Rbc} &= RI_{bc} \\ V_{Rca} &= RI_{ca} \end{aligned} \tag{4.9}$$

Substituting equations 4.8 and 4.9 into equation 4.7 results in the following expression

$$\begin{aligned} V_{ab} &= L\frac{dI_{ab}}{dt} + D_{ab}V_i + RI_{ab} \\ V_{bc} &= L\frac{dI_{bc}}{dt} + D_{bc}V_i + RI_{bc} \\ V_{ca} &= L\frac{dI_{ca}}{dt} + D_{ca}V_i + RI_{ca} \end{aligned} \tag{4.10}$$

Multiplying both sides of equation 4.10 by $\frac{1}{\sqrt{3}}$ results in

$$
\begin{aligned}
\frac{1}{\sqrt{3}}V_{ab} &= \frac{1}{\sqrt{3}}L\frac{dI_{ab}}{dt} + \frac{1}{\sqrt{3}}D_{ab}V_i + \frac{1}{\sqrt{3}}RI_{ab} \\
\frac{1}{\sqrt{3}}V_{bc} &= \frac{1}{\sqrt{3}}L\frac{dI_{bc}}{dt} + \frac{1}{\sqrt{3}}D_{bc}V_i + \frac{1}{\sqrt{3}}RI_{bc} \\
\frac{1}{\sqrt{3}}V_{ca} &= \frac{1}{\sqrt{3}}L\frac{dI_{ca}}{dt} + \frac{1}{\sqrt{3}}D_{ca}V_i + \frac{1}{\sqrt{3}}RI_{ca}
\end{aligned}
\tag{4.11}
$$

Equation 4.11 can be represented vectorially as

$$
\vec{V}_{abc} = L\frac{d\vec{I}_{abc}}{dt} + \vec{D}_{abc}V_i + R\vec{I}_{abc} \tag{4.12}
$$

where

$$
\vec{V}_{abc} = \frac{1}{\sqrt{3}}\begin{bmatrix} V_{ab} \\ V_{bc} \\ V_{ca} \end{bmatrix}, \qquad \vec{I}_{abc} = \frac{1}{\sqrt{3}}\begin{bmatrix} I_{ab} \\ I_{bc} \\ I_{ca} \end{bmatrix} \text{ and } \qquad \vec{D}_{abc} = \frac{1}{\sqrt{3}}\begin{bmatrix} D_{ab} \\ D_{bc} \\ D_{ca} \end{bmatrix} \tag{4.13}
$$

Now that the system in figure 4.3 has been described vectorially, the dq0-transformation can be used to obtain the system's representation in the dq0 domain. From equations 2.20-2.22, the vectors $\vec{V}_{abc}$, $\vec{I}_{abc}$ and $\vec{D}_{abc}$ can be rewritten as

$$
\begin{aligned}
\vec{V}_{abc} &= P^{-1}\vec{V}_{dq0} \\
\vec{I}_{abc} &= P^{-1}\vec{I}_{dq0} \\
\vec{D}_{abc} &= P^{-1}\vec{D}_{dq0}
\end{aligned}
\tag{4.14}
$$

Substituting these terms in equation 4.13 results in

$$P^{-1}\vec{V}_{dq0} = L\frac{d[P^{-1}\vec{I}_{dq0}]}{dt} + P^{-1}\vec{D}_{dq0}V_i + RP^{-1}\vec{I}_{dq0} \tag{4.15}$$

Multiplying equation 4.15 on the left by the transformation matrix P leads to

$$\vec{V}_{dq0} = LP\frac{d[P^{-1}\vec{I}_{dq0}]}{dt} + \vec{D}_{dq0}V_i + R\vec{I}_{dq0} \tag{4.16}$$

The derivative term $P\frac{d[P^{-1}\vec{I}_{dq0}]}{dt}$ can be solved as follows

$$\begin{aligned}
P\frac{d[P^{-1}\vec{I}_{dq0}]}{dt} &= P\frac{dP^{-1}}{dt}\vec{I}_{dq0} + \frac{d\vec{I}_{dq0}}{dt} \\
&= \sqrt{\frac{2}{3}}P\frac{d}{dt}\begin{bmatrix} \cos(\omega t) & -\sin(\omega t) & \frac{1}{\sqrt{2}} \\ \cos(\omega t - \frac{2\pi}{3}) & -\sin(\omega t - \frac{2\pi}{3}) & \frac{1}{\sqrt{2}} \\ \cos(\omega t + \frac{2\pi}{3}) & -sin(\omega t + \frac{2\pi}{3}) & \frac{1}{\sqrt{2}} \end{bmatrix}\vec{I}_{dq0} + \frac{d\vec{I}_{dq0}}{dt} \\
&= \sqrt{\frac{2}{3}}\omega P\begin{bmatrix} -\sin(\omega t) & -\cos(\omega t) & 0 \\ -\sin(\omega t - \frac{2\pi}{3}) & -\cos(\omega t - \frac{2\pi}{3}) & 0 \\ -\sin(\omega t + \frac{2\pi}{3}) & -\cos(\omega t + \frac{2\pi}{3}) & 0 \end{bmatrix}\vec{I}_{dq0} + \frac{d\vec{I}_{dq0}}{dt} \\
&= \omega\begin{bmatrix} 0 & -1 & 0 \\ 1 & 0 & 0 \\ 0 & 0 & 0 \end{bmatrix}\vec{I}_{dq0} + \frac{d\vec{I}_{dq0}}{dt}
\end{aligned} \tag{4.17}$$

Then, equation 4.16 becomes

$$\vec{V}_{dq0} = L\frac{d\vec{I}_{dq0}}{dt} + L\omega \begin{bmatrix} 0 & -1 & 0 \\ 1 & 0 & 0 \\ 0 & 0 & 0 \end{bmatrix} \vec{I}_{dq0} + \vec{D}_{dq0}V_i + R\vec{I}_{dq0}$$

$$\begin{bmatrix} V_d \\ V_q \\ V_0 \end{bmatrix} = L \begin{bmatrix} \frac{d\vec{I}_d}{dt} \\ \frac{d\vec{I}_q}{dt} \\ \frac{d\vec{I}_0}{dt} \end{bmatrix} + L\omega \begin{bmatrix} -I_q \\ I_d \\ 0 \end{bmatrix} + \begin{bmatrix} D_q \\ D_d \\ D_0 \end{bmatrix} V_i + R \begin{bmatrix} I_d \\ I_q \\ I_0 \end{bmatrix} \tag{4.18}$$

It is important to note $V_{ab} + V_{bc} + V_{ca} = I_{ab} + I_{bc} + I_{ca} = D_{ab} + D_{bc} + D_{ca} = 0$. Therefore all the zero components, that is, V_0, I_0 and D_0 are null and the last line in equation 4.18 can be disregarded. Applying the dq0-transformation to the line voltages defined in equation 4.3 results in

$$\begin{aligned} V_d &= \sqrt{\frac{3}{2}}V_{ph} \\ V_q &= 0 \end{aligned} \tag{4.19}$$

Substituting equation 4.19 into equation 4.18 leads to the following equations.

$$\begin{aligned} \sqrt{\frac{3}{2}}V_{ph} = L\frac{dI_d}{dt} - L\omega I_q + D_dV_i + RI_d &\Longrightarrow \frac{dI_d}{dt} = \sqrt{\frac{3}{2}}\frac{V_{ph}}{L} + \omega I_q - \frac{V_i}{L}D_d - \frac{R}{L}I_d \\ 0 = L\frac{dI_q}{dt} + L\omega I_d + D_qV_i + RI_q &\Longrightarrow \frac{dI_q}{dt} = -\omega I_d - \frac{V_i}{L}D_q - \frac{R}{L}I_q \end{aligned} \tag{4.20}$$

Figure 4.4 shows the equivalent circuits corresponding to equation 4.20.

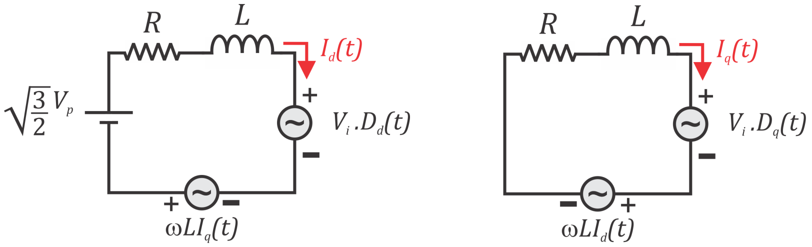

Figure 4.4: Equivalent circuits in the dq0 domain.

It can be seen that the circuits shown above are coupled, that is, the differential equation describing $\mathrm{I_d}$ depends on $\mathrm{I_q}$ and vice versa. In order to decouple those equations a new duty cycle is defined as follows

$$\begin{aligned} D'_d &= D_d - \frac{\omega L}{V_i} I_q \\ D'_q &= D_q + \frac{\omega L}{V_i} I_d \end{aligned} \tag{4.21}$$

Substituting equation 4.21 into equation 4.20 results in

$$\begin{aligned} \frac{dI_d}{dt} &= \sqrt{\frac{3}{2}}\frac{V_{ph}}{L} - \frac{V_i}{L}D'_d - \frac{R}{L}I_d \\ \frac{dI_q}{dt} &= -\frac{V_i}{L}D'_q - \frac{R}{L}I_q \end{aligned} \tag{4.22}$$

Each of the circuit variables can be described as a composition of an AC function corresponding to its harmonic content and a DC function corresponding to its average value.

$$
\begin{aligned}
I_d &= \overline{I}_d + \widetilde{i}_d \\
I_q &= \overline{I}_q + \widetilde{i}_q \\
D'_d &= \overline{D}'_d + \widetilde{d}'_d \\
D'_q &= \overline{D}'_q + \widetilde{d}'_q
\end{aligned}
\tag{4.23}
$$

Replacing I_d, I_q, D'_d and D'_q in equation 4.22 by the expressions in equation 4.23 gives the following result

$$
\begin{aligned}
\frac{d}{dt}[\overline{I}_d + \widetilde{i}_d] &= \sqrt{\frac{3}{2}}\frac{V_{ph}}{L} - \frac{V_i}{L}[\overline{D}'_d + \widetilde{d}'_d] - \frac{R}{L}[\overline{I}_d + \widetilde{i}_d] \\
\frac{d}{dt}[\overline{I}_q + \widetilde{i}_q] &= -\frac{V_i}{L}[\overline{D}'_q + \widetilde{d}'_q] - \frac{R}{L}[\overline{I}_q + \widetilde{i}_q]
\end{aligned}
\tag{4.24}
$$

Next, the AC signals are zeroed and the circuit is analyzed in its operating point. At the operating point the current derivative is 0, which leads to

$$
\begin{aligned}
\overline{D}'_d &= \sqrt{\frac{3}{2}}\frac{V_{ph}}{V_i} - \frac{R}{V_i}\overline{I}_d \\
\overline{D}'_q &= -\frac{R}{V_i}\overline{I}_q
\end{aligned}
\tag{4.25}
$$

Equation 4.25 can then be substituted into equation 4.24 resulting in equation 4.26

$$
\begin{aligned}
\frac{d\widetilde{i}_d}{dt} &= -\frac{V_i}{L}\widetilde{d}'_d - \frac{R}{L}\widetilde{i}_d \\
\frac{d\widetilde{i}_q}{dt} &= -\frac{V_i}{L}\widetilde{d}'_q - \frac{R}{L}\widetilde{i}_q
\end{aligned}
\tag{4.26}
$$

Finally, applying Laplace transform to equation 4.26 results in two transfer functions relating the direct and quadrature currents to its respective duty cycles.

$$\begin{aligned} \frac{\widetilde{i}_d(s)}{\widetilde{d}'_d(s)} &= -\frac{V_i}{sL+R} \\ \frac{\widetilde{i}_q(s)}{\widetilde{d}'_q(s)} &= -\frac{V_i}{sL+R} \end{aligned} \tag{4.27}$$

Equation 4.27 gives the model which is being looked for. The model provides the signals $\widetilde{d}'_d(s)$ and $\widetilde{d}'_q(s)$ necessary to control the current in the d and q axes. Those signals must be used in equation 4.21 in order to determine $\widetilde{d}_d(s)$ and $\widetilde{d}_q(s)$. Then, it is important to remember that the inverse dq0-transformation of $\widetilde{d}_d(s)$ and $\widetilde{d}_q(s)$ gives the line duty cycles $\mathrm{D_{ab}}$, $\mathrm{D_{bc}}$ and $\mathrm{D_{ca}}$. However, in order to perform the PWM modulation, $\mathrm{D_a}$, $\mathrm{D_b}$ and $\mathrm{D_c}$ must be used instead. It can be easily shown that

$$\begin{bmatrix} D_a \\ D_b \\ D_c \end{bmatrix} = \begin{bmatrix} \frac{1}{3} & 0 & -\frac{1}{3} \\ -\frac{1}{3} & \frac{1}{3} & 0 \\ 0 & -\frac{1}{3} & \frac{1}{3} \end{bmatrix} \begin{bmatrix} D_{ab} \\ D_{bc} \\ D_{ca} \end{bmatrix} \tag{4.28}$$

Thus, after doing the matrix multiplication shown in equation 4.28, the output signal can be used in the modulation process.

4.1.2 The model for voltage control

The next step is to develop a model for voltage control. The objective is to control the voltage across the capacitor $\mathrm{C_i}$ in order to track the PV panel maximum power point.

Section 3.3 presented three different techniques commonly used to extract maximum power from a PV panel. In the system reported in this document two of them will be used in combination, namely, the constant voltage method and the perturb and observe algorithm. The reason for that is the following: the converter must be operative even in a no-light condition, when it still will be doing harmonic compensation. In order to work as an active filter, the capacitor $\mathrm{C_i}$ must be charged. If only the perturb and observe algorithm is used, it will drive the capacitor voltage to zero in the absence of sunlight making the active filter to fail. If only the constant voltage method is applied, then the system will not be tracking the maximum power point, which means sub-optimum operation, especially in face of temperature and radiance changes. By combining the two techniques the capacitor is guaranteed to stay charged when the sunlight is not reaching the panel. The maximum power point will be tracked otherwise.

In order to implement the aforesaid control scheme it is necessary to find a relationship between the input voltage $\mathrm{V_i}$ and the direct-axis current $\mathrm{i_d}$. That is done developing a model for the converter as seen from the DC link. From figure 4.2 it can be seen that.

$$I_i = I_aD_a + I_bD_b + I_cD_c = \frac{1}{\sqrt{3}}\begin{bmatrix} I_{ab} & I_{ab} & I_{ab} \end{bmatrix} \cdot \frac{1}{\sqrt{3}}\begin{bmatrix} D_{ab} \\ D_{ab} \\ D_{ab} \end{bmatrix} \tag{4.29}$$

which can be written in vectorial form as

$$I_i = \vec{I}^T_{abc}.\vec{D}_{abc} \tag{4.30}$$

From equation 2.21 it can be verified that the dq0 transformation matrix is orthogonal, that is, $P^{-1} = P^T$. Consequently, $[P^{-1}]^T = P$. The transpose of dq0 current vector can then be written as

$$\vec{I}^{T}_{dq0} = (P\vec{I}_{abc})^{T} = \vec{I}^{T}_{abc}P^{T} = \vec{I}^{T}_{abc}P^{-1} \tag{4.31}$$

Thus, equation 4.30 can be rewritten as follows

$$I_i = \vec{I}^{T}_{abc}[P^{-1}P].\vec{D}_{abc} = \vec{I}^{T}_{dq0}\vec{D}_{dq0} = I_d D_d + I_q D_q \tag{4.32}$$

Figure 4.5 shows the converter equivalent circuit as seen from the input side.

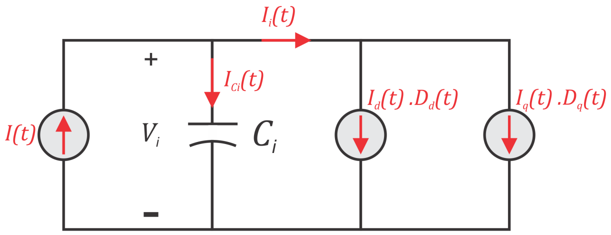

Figure 4.5: Converter equivalent circuit as seen from the DC side.

I(t) represents the current provided by the PV array. From the last figure it can be seen that

$$I = I_{Ci} + I_i = C_i\frac{dV_i}{dt} + I_i \tag{4.33}$$

Each one of the variables shown above can be described as a superposition of an AC function on a DC function, with the former representing the current harmonics and the latter the current average.

$$\begin{aligned} I_i &= \overline{I}_i + \widetilde{i}_i \\ I &= \overline{I} + \widetilde{i} \\ I_{Ci} &= \overline{I}_{Ci} + \widetilde{i}_{Ci} \\ V_i &= \overline{V}_i + \widetilde{v}_i \end{aligned} \tag{4.34}$$

Substituting equation 4.34 into equation 4.33 results in

$$\overline{I} + \widetilde{i} = \overline{I}_{Ci} + \widetilde{i}_{Ci} + \overline{I}_i + \widetilde{i}_i \tag{4.35}$$

Next, the AC signals are zeroed and the circuit is analyzed in its operating point. At the operating point the capacitor current is 0, which leads to

$$\overline{I} = \overline{I}_i \tag{4.36}$$

Substituting the previous equation into equation 4.35 leads to

$$\widetilde{i} = \widetilde{i}_{Ci} + \widetilde{i}_i = C_i \frac{d\widetilde{v}_i}{dt} + \widetilde{i}_i \tag{4.37}$$

Applying the Laplace transform to equation 4.37 results in the following equation

$$\widetilde{i}(s) = sC_i\widetilde{v}_i(s) + \widetilde{i}_i(s) \tag{4.38}$$

The transfer function between the input voltage v_i and the current i_i is given by

$$\frac{\widetilde{v}_i(s)}{\widetilde{i}_i(s)} = -\frac{1}{sC_i} \tag{4.39}$$

Equation 4.39 describes the relationship between the input voltage and the input current. However, the information being searched for is the relation of $\mathrm{v_i}$ to the direct-axis current $\mathrm{i_d}$. In order to go from the first to the second, equation 4.32 is considered again. $\mathrm{I_i}$, $\mathrm{I_d}$, $\mathrm{I_q}$, $\mathrm{D_d}$ and $\mathrm{D_q}$ can also be described as a superposition of an AC function on a DC function.

$$\begin{aligned}
I_i &= \overline{I}_i + \widetilde{i}_i \\
I_d &= \overline{I_d} + \widetilde{i}_d \\
I_q &= \overline{I_q} + \widetilde{i}_q \\
D_d &= \overline{D_d} + \widetilde{d}_d \\
D_q &= \overline{D_q} + \widetilde{d}_q
\end{aligned} \tag{4.40}$$

Substituting equation 4.40 into equation 4.32 results in

$$\begin{aligned}
\overline{I}_i + \widetilde{i}_i &= (\overline{I}_d + \widetilde{i}_d)(\overline{D}_d + \widetilde{d}_d) + (\overline{I}_q + \widetilde{i}_q)(\overline{D}_q + \widetilde{d}_q) \\
\overline{I}_i + \widetilde{i}_i &= \overline{I}_d\overline{D}_d + \overline{I}_d\widetilde{d}_d + \widetilde{i}_d\overline{D}_d + \widetilde{i}_d\widetilde{d}_d + \overline{I}_q\overline{D}_q + \overline{I}_q\widetilde{d}_q + \widetilde{i}_q\overline{D}_q + \widetilde{i}_q\widetilde{d}_q
\end{aligned} \tag{4.41}$$

It will be assumed that the products of the AC signals shown in equation 4.41 are negligible, such that the equation can be rewritten as

$$\overline{I}_i + \widetilde{i}_i = (\overline{I}_d\overline{D}_d + \overline{I}_q\overline{D}_q) + (\overline{I}_d\widetilde{d}_d + \widetilde{i}_d\overline{D}_d + \overline{I}_q\widetilde{d}_q + \widetilde{i}_q\overline{D}_q) \tag{4.42}$$

From equation 4.42 it can be seen that

$$\widetilde{i}_i = \overline{I}_d \widetilde{d}_d + \widetilde{i}_d \overline{D}_d + \overline{I}_q \widetilde{d}_q + \widetilde{i}_q \overline{D}_q \tag{4.43}$$

Applying the Laplace transform to the last equation leads to

$$\widetilde{i}_i(s) = \overline{I}_d \widetilde{d}_d(s) + \widetilde{i}_d(s) \overline{D}_d + \overline{I}_q \widetilde{d}_q(s) + \widetilde{i}_q(s) \overline{D}_q \tag{4.44}$$

The converter output power can be written in terms of average components as follows

$$\begin{aligned} \overline{P} &= \overline{V}_d \overline{I}_d + \overline{V}_q \overline{I}_q \\ \overline{Q} &= \overline{V}_q \overline{I}_d - \overline{V}_d \overline{I}_q \end{aligned} \tag{4.45}$$

From equation 4.19 it is already known that $\overline{V}_q = 0$. Thus, equation 4.45 can be simplified as shown below.

$$\begin{aligned} \overline{P} &= \overline{V}_d \overline{I}_d \\ \overline{Q} &= -\overline{V}_d \overline{I}_q \end{aligned} \tag{4.46}$$

It follows that the currents I_d and I_q can be written as

$$\begin{aligned} \overline{I}_d &= \frac{\overline{P}}{\overline{V}_d} = \sqrt{\frac{2}{3}} \frac{\overline{P}}{V_{ph}} \\ \overline{I}_q &= -\frac{\overline{Q}}{\overline{V}_d} = -\sqrt{\frac{2}{3}} \frac{\overline{Q}}{V_{ph}} \end{aligned} \tag{4.47}$$

To obtain the duty cycles D_d and D_q, equation 4.20 is analyzed at the operational point, where the derivatives are zero.

$$
\begin{aligned}
0 &= LL\omega\overline{I}_q + \sqrt{\frac{3}{2}}\frac{V_{ph}}{-}\frac{V_i}{L}D_d - \frac{R}{L}\overline{I}_d \\
0 &= -\frac{V_i}{L}D_q - \frac{R}{L}\overline{I}_q
\end{aligned}
\tag{4.48}
$$

That leads to the following result

$$
\begin{aligned}
D_d &= \frac{L\omega}{V_i}\overline{I}_q + \sqrt{\frac{3}{2}}\frac{V_{ph}}{V_i} - \frac{R}{V_i}\overline{I}_d \\
D_q &= -\frac{L\omega}{V_i}\overline{I}_d - \frac{R}{V_i}\overline{I}_q
\end{aligned}
\tag{4.49}
$$

Now, equations 4.47 and 4.49 are combined with equation 4.44, resulting in the following expression

$$
\begin{aligned}
\widetilde{i}_i(s) =& \sqrt{\frac{2}{3}}\frac{\overline{P}}{V_{ph}}\widetilde{d}_d(s) + \widetilde{i}_d(s)(\sqrt{\frac{3}{2}}\frac{V_{ph}}{V_i} - \sqrt{\frac{2}{3}}\frac{\omega L}{V_{ph}V_i}\overline{Q} - \sqrt{\frac{2}{3}}\frac{R}{V_{ph}V_i}\overline{P}) \\
&- \sqrt{\frac{2}{3}}\frac{\overline{Q}}{V_{ph}}\widetilde{d}_q(s) + \widetilde{i}_q(s)\sqrt{\frac{2}{3}}(\frac{R}{V_{ph}V_i}\overline{Q} - \frac{\omega L}{V_{ph}V_i}\overline{P})
\end{aligned}
\tag{4.50}
$$

From equation 4.27 it follows that

$$
\begin{aligned}
\widetilde{d}'_d &= -\frac{sL + R}{V_i}\widetilde{i}_d(s) \\
\widetilde{d}'_q &= -\frac{sL + R}{V_i}\widetilde{i}_q(s)
\end{aligned}
\tag{4.51}
$$

Replacing equation 4.21 into equation 4.51 results in the following equation

$$
\begin{aligned}
\widetilde{d}_d &= \frac{\omega L}{V_i}\widetilde{i}_q - \frac{sL + R}{V_i}\widetilde{i}_d(s) \\
\widetilde{d}_q &= \frac{\omega L}{V_i}\widetilde{i}_d - \frac{sL + R}{V_i}\widetilde{i}_q(s)
\end{aligned}
\tag{4.52}
$$

Next, equation 4.52 is combined with equation 4.50 to give the relationship between

i_i, i_d and i_q. The result is shown in equation 4.53.

$$\widetilde{i}_i(s) = \left[\sqrt{\frac{2}{3}}\frac{\overline{LP}}{V_{ph}V_i}s - \sqrt{\frac{2}{3}}\frac{\overline{2RP}}{V_{ph}V_i} + \sqrt{\frac{3}{2}}\frac{V_{ph}}{V_i}\right]\widetilde{i}_d(s) + \left[\sqrt{\frac{2}{3}}\frac{LQ}{V_{ph}V_i}s + \sqrt{\frac{2}{3}}\frac{2RQ}{V_{ph}V_i}\right]\widetilde{i}_q(s) \tag{4.53}$$

From the equation above it can be seen that

$$\begin{aligned} \frac{\widetilde{i}_i(s)}{\widetilde{i}_d(s)} &= \sqrt{\frac{2}{3}}\frac{\overline{LP}}{V_{ph}V_i}s - \sqrt{\frac{2}{3}}\frac{\overline{2RP}}{V_{ph}V_i} + \sqrt{\frac{3}{2}}\frac{V_{ph}}{V_i} \\ \frac{\widetilde{i}_i(s)}{\widetilde{i}_q(s)} &= \sqrt{\frac{2}{3}}\frac{LQ}{V_{ph}V_i}s + \sqrt{\frac{2}{3}}\frac{2RQ}{V_{ph}V_i} \end{aligned} \tag{4.54}$$

Last, the desired transfer function is found by combining equations 4.39 and 4.54

$$\begin{aligned} \frac{\widetilde{v}_i(s)}{\widetilde{i}_d(s)} &= \frac{\widetilde{v}_i(s)}{\widetilde{i}_i(s)}\frac{\widetilde{i}_i(s)}{\widetilde{i}_d(s)} = -\frac{1}{sC_i}\left[\sqrt{\frac{2}{3}}\frac{L\overline{P}}{V_{ph}V_i}s - \sqrt{\frac{2}{3}}\frac{2R\overline{P}}{V_{ph}V_i} + \sqrt{\frac{3}{2}}\frac{V_{ph}}{V_i}\right] \\ \frac{\widetilde{v}_i(s)}{\widetilde{i}_q(s)} &= \frac{\widetilde{v}_i(s)}{\widetilde{i}_i(s)}\frac{\widetilde{i}_i(s)}{\widetilde{i}_q(s)} = -\frac{1}{sC_i}\left[\sqrt{\frac{2}{3}}\frac{L\overline{Q}}{V_{ph}V_i}s + \sqrt{\frac{2}{3}}\frac{2R\overline{Q}}{V_{ph}V_i}\right] \end{aligned} \tag{4.55}$$

This chapter presented the converter modeling for current and voltage control. In the next chapter a control system will be designed based on the models obtained here.

5. CONVERTER AND COMPENSATION SYSTEM DESIGN

Now that the converter models for current and voltage control have been developed, a control system will be designed in order to make the actual converter to behave in the expected way.

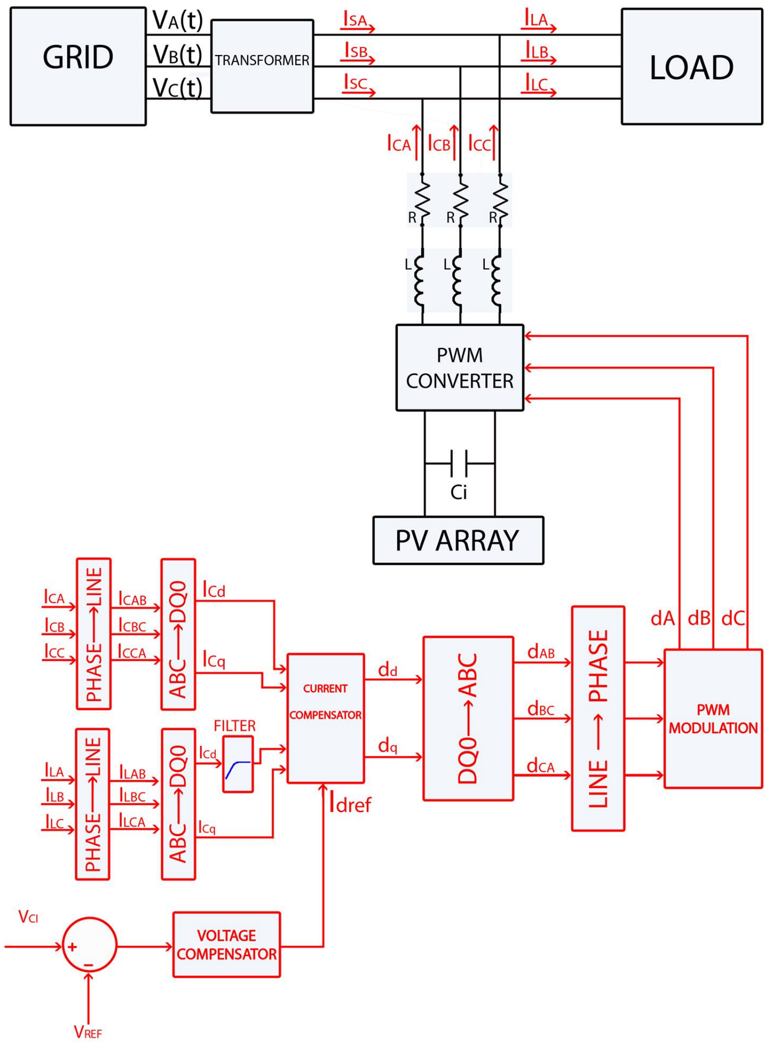

Figure 5.1: System configuration including the control module

Figure 5.1 shows a schematic representation of the whole system. The control strategy adopted here is very close to the one described in section 2.2.2. There is an inner and an outer control loop in cascade working together to control the converter output current and the capacitor voltage at the same time. A maximum power point tracking algorithm (not shown) is implemented to provide the reference voltage. The load currents, the converter output currents, the input voltage and current are measured. The voltage controller takes the reference and the measured voltage signals as inputs and generate a d-axis reference current that is fed into the current controller. The load and converter currents are converted to the dq0 domain and the real and imaginary instantaneous power are determined. The instantaneous real power signal goes through a low-pass filter in order to eliminate its AC components. The resultant signals $\overline{p}$ and q are used to generate current references to the control loop. These signals are combined with the other current reference generated by the voltage controller and fed into the current controller, which generates the duty cycles signals used in the PWM modulation circuit.

The next sections will present the system that will be simulated and provide more details about each of the steps described above.

5.1 System specifications

Table 5.1 presents a few system specifications. P is the power processed by the converter, $\mathrm{V_{out}}$ is the converter output voltage, which is the same as the grid voltage, $\mathrm{f_G}$ is the grid voltage frequency, $\mathrm{f_s}$ is the sampling frequency, $\mathrm{K_c}$ is the current sensor gain, $\mathrm{K_v}$ the voltage sensor gain and η is the converter efficiency. The simulations will be carried out using a model for the KC200GT PV panel, manufactured by the company Kyocera. Table 5.2 shows the electrical properties of the PV panel[14].

The converter is designed to handle a rated power of 12 kVA. If 57 panels are employed in 3 parallel strings of 19 panels each, the maximum power provided by the array is $P_{pv} = 57 \times 200 = 11.4\ kW$. The voltage across each parallel string at the maximum power point is $V_{pv} = 19 \times 26.3 = 499.7\ V \approx 500\ V$. The total output current at the maximum power point is $I_{pv} = 3 \times 7.61 = 22.8\ A$.

Table 5.1: System specifications

P = 12 kVA
$\mathrm{V_{out}} = 120$ V
$f_g = 60$ Hz
$f_s = 20$ kHz
$\mathrm{K_c} = 0.1$
$\mathrm{K_v} = 0.01$
$\Delta i_{Lmax} = 0.04\mathrm{I_{peak}}$
$\Delta V_{ciH} = 0.1\mathrm{V_i}$
$\Delta t_{hold} = 5.5$ ms

Table 5.2: Electrical properties of PV panel KC200GT

Parameter	**Value**
Maximum power at standard test conditions	200 W
MPP voltage (V_{mpp})	26.3 V
MPP Current (I_{mpp})	7.61 A
Open circuit voltage (V_{oc})	32.9 V
Short circuit current (I_{sc})	8.21 A

5.1.1 Output inductors specification

In order to determine the value of the output inductors L_1, L_2 and L_3, it is necessary to know the voltage applied across each one of them. That can be done analyzing the so called *topological states*[6] of the converter shown in figure 4.1, which is shown again in figure 5.2 for convenience.

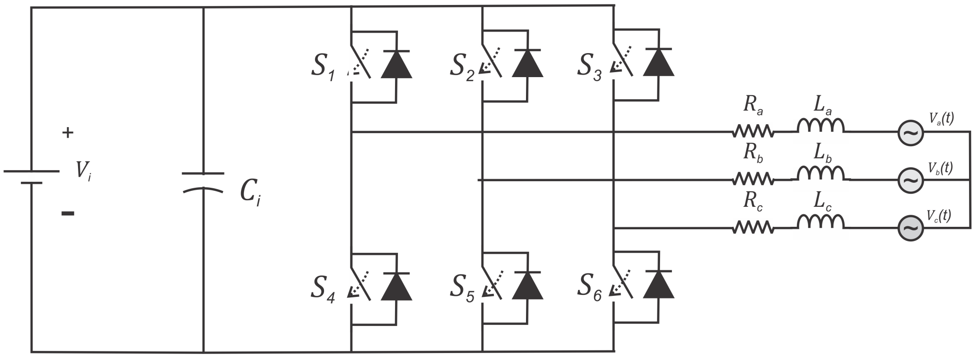

Figure 5.2: System schematic representation.

In general, the topological states of a converter depend not only on the switches states, but also on the current flow directions. Each current can flow in two different directions. Since there are three converter currents, there would be in principle $2^3 = 8$ different current flow patterns. However, for the three-phase three wire converter considered here, $i_a(t) + i_b(t) + i_c(t) = 0$, which means that the three currents cannot flow in the same direction simultaneously. Therefore, two of those eight patterns must be disregarded leaving six to be considered.

Figure 5.3 shows the converter output currents during one cycle. The dashed vertical lines show the six sections of the graph that correspond to the six current flow patterns to be analyzed. Section 2 ($60° \leq \theta \leq 120°$) is going to be considered in the analysis and the results will be generalized. In that section, $\mathrm{i_a}$(t) is positive (flowing in the converter) while $\mathrm{i_b}$(t) and $\mathrm{i_c}$(t) are both negatives (flowing out the converter).

A switch state is “on” if the switch is closed and “off” otherwise. The switches in a branch are complementary to each other, that is, if one in on, the other is necessarily off. For instance, if $\mathrm{S_1}$ is on, then $\mathrm{S_4}$ is off and vice-versa. Figures 5.4-5.7 show the eight possible topological states that correspond to the current direction of section 2 in figure 5.3.

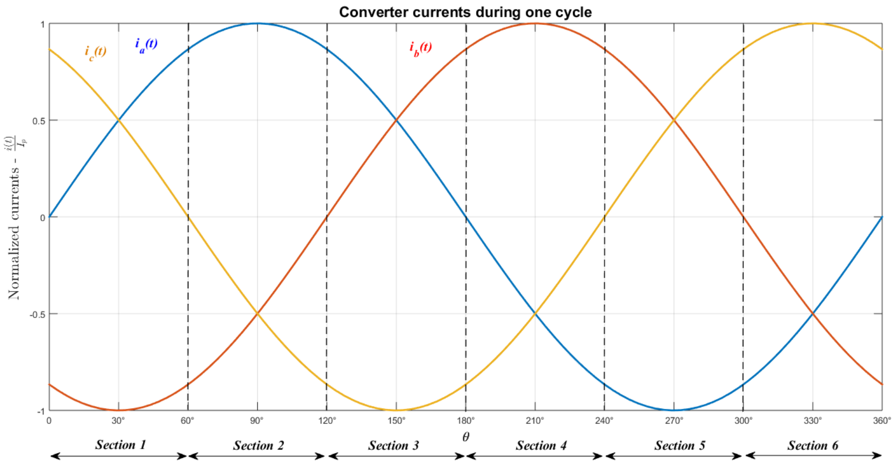

Figure 5.3: Converter phase currents in one cycle.

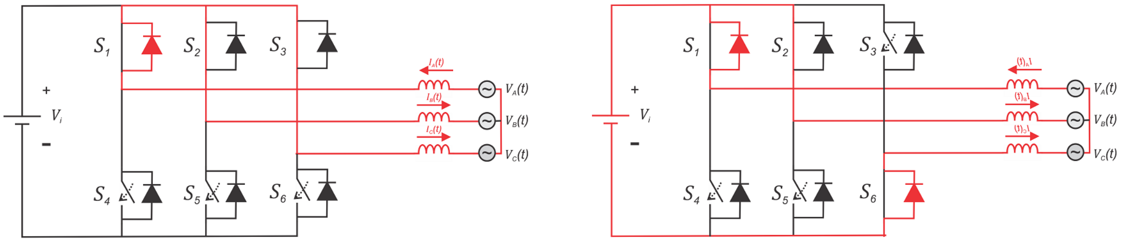

STATE 1: S1 ON - S2 ON - S3 ON

STATE 2: S1 ON - S2 ON - S3 OFF

Figure 5.4: Topological states 1 and 2.

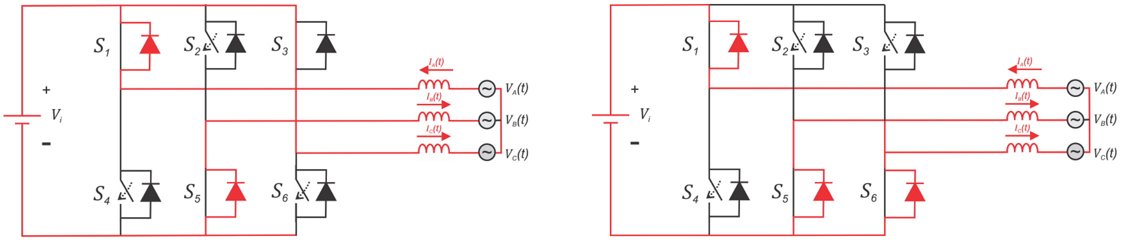

STATE 3: S1 ON - S2 OFF - S3 ON

STATE 4: S1 ON - S2 OFF - S3 OFF

Figure 5.5: Topological states 3 and 4.

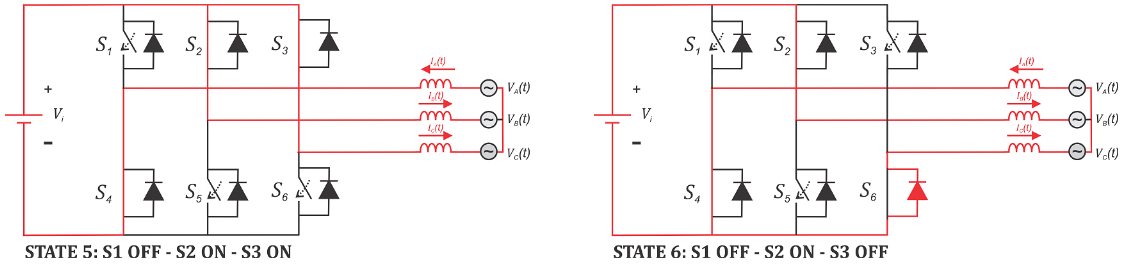

STATE 5: S1 OFF - S2 ON - S3 ON

STATE 6: S1 OFF - S2 ON - S3 OFF

Figure 5.6: Topological states 5 and 6.

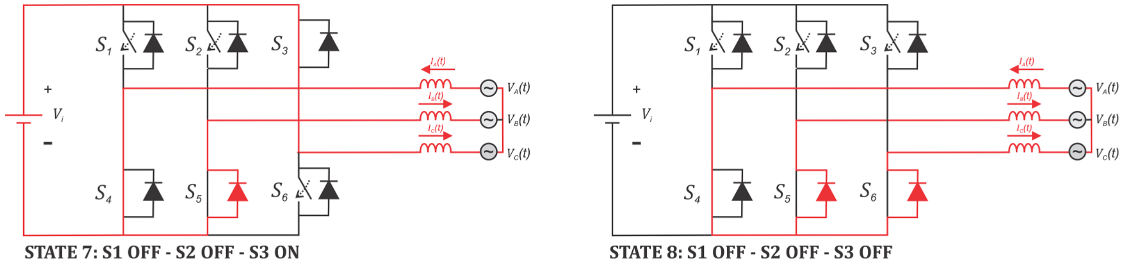

STATE 7: S1 OFF - S2 OFF - S3 ON

STATE 8: S1 OFF - S2 OFF - S3 OFF

Figure 5.7: Topological states 7 and 8.

Figure 5.8 shows the duty cycles over section 2. In the range $60° \leq \theta \leq 90°$, the duty cycle "a" is greater than duty cycle "c" which in turn is greater than duty cycle

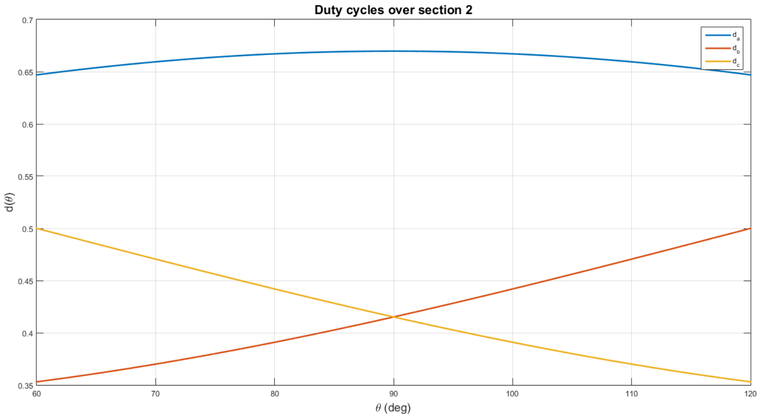

Figure 5.8: Duty cycle over section 2.

"b", that is

$$d_a(t) \geq d_c(t) \geq d_b(t) \tag{5.1}$$

Analyzing the topological states shown in figures 5.4-5.7 it can be seen that only four of them can possibly satisfy the condition expressed by equation 5.1, namely, states 1, 3, 4 and 8. It is assumed that state 1 lasts for t_1 seconds, state 3 for t_3 seconds and so on. Table 5.3 shows each topological state with its correspondent duration and switch configuration, while figure 5.9 presents the same information graphically. From figure 5.9 it can be seen that

$$\begin{aligned} t_1 &= T_s d_b \\ t_3 &= T_s(d_c - d_b) \\ t_4 &= T_s(d_a - d_c) \\ t_8 &= T_s(1 - d_a) \end{aligned} \tag{5.2}$$

Tables 5.4 and 5.5 show the voltage across each inductor and the derivative sign of each inductor current in the topological states being considered here.

Table 5.3: Topological states that meet the condition expressed in equation 5.1 with its respective durations and switch configurations

Time duration	Topological state	switches		
		S_1	S_2	S_3
t_1	1	ON	ON	ON
t_3	3	ON	OFF	ON
t_4	4	ON	OFF	OFF
t_8	8	OFF	OFF	OFF

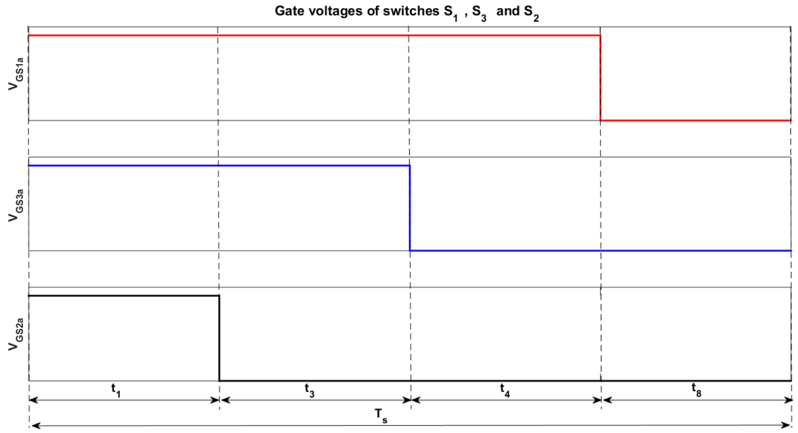

Figure 5.9: Gate voltages of switches S_1, S_3 and S_2.

Table 5.4: Voltage across the ouput inductors

Topological state	Voltage		
	$V_{La}(t)$	$V_{Lb}(t)$	$V_{Lc}(t)$
1	$V_a(t)$	$V_b(t)$	$V_c(t)$
3	$V_a(t)-\frac{V_i}{3}$	$V_b(t)+\frac{2V_i}{3}$	$V_c(t)-\frac{V_i}{3}$
4	$V_a(t)-\frac{2V_i}{3}$	$V_b(t)+\frac{V_i}{3}$	$V_c(t)+\frac{V_i}{3}$
8	$V_a(t)$	$V_b(t)$	$V_c(t)$

The inductor voltage is given by

$$V_L = L\frac{di_L}{dt} \approx L\frac{\Delta i_L}{\Delta t} \tag{5.3}$$

From table 5.5 it can be seen that the current variation in inductor “a” is positive for all the states but state 4. The duration of state 4 is shown in equation 5.2. Table 5.4 shows the voltage across inductor “a” in state 4. Substituting those expressions

Table 5.5: Current derivatives

Topological state	Current derivative		
	$\frac{di_a(t)}{dt}$	$\frac{di_b(t)}{dt}$	$\frac{di_c(t)}{dt}$
1	> 0	< 0	< 0
3	>0, if $V_a(t) > \frac{V_i}{3}$ <0, if $V_a(t) < \frac{V_i}{3}$	>0	<0
4	<0	>0, if $V_b(t) > -\frac{V_i}{3}$ <0, if $V_c(t) < -\frac{V_i}{3}$	>0, if $V_b(t) > -\frac{V_i}{3}$ <0, if $V_c(t) < -\frac{V_i}{3}$
8	> 0	< 0	< 0

into equation 5.3 results in

$$V_a(t) - \frac{2V_i}{3} = L_a \frac{\Delta i_{La}}{T_s(d_a - d_c)} \Rightarrow L_a \Delta i_{La} f_s = [d_a(t) - d_c(t)][V_a(t) - \frac{2V_i}{3}] \tag{5.4}$$

In an analogous way it can be shown that

$$\begin{aligned} L_b \Delta i_{Lb} f_s &= [d_c(t) - d_b(t)][V_b(t) + \frac{2V_i}{3}] \\ L_c \Delta i_{Lc} f_s &= [d_a(t) - d_c(t)][V_c(t) + \frac{V_i}{3}] \end{aligned} \tag{5.5}$$

Figure 5.10 shows a graphical representation of the parametric currents shown in equations 5.4 and 5.5. It can be seen that the greatest variation in absolute value occurs at $\omega t = 90^\circ$ for $L_a \Delta i_{La} f_s$. From equation 5.4 follows that

$$\begin{aligned} L_a \Delta i_{Lamax} f_s &= \frac{V_p}{V_i}[\sin(\frac{pi}{2}) - \sin(\frac{7\pi}{6})][V_p \sin(\frac{\pi}{2}) - \frac{2V_i}{3}] \\ L_a \Delta i_{Lamax} f_s &= \frac{V_p}{V_i}[V_i - 1.5V_p] \end{aligned} \tag{5.6}$$

It is assumed that the three inductors have the same inductance and are subject

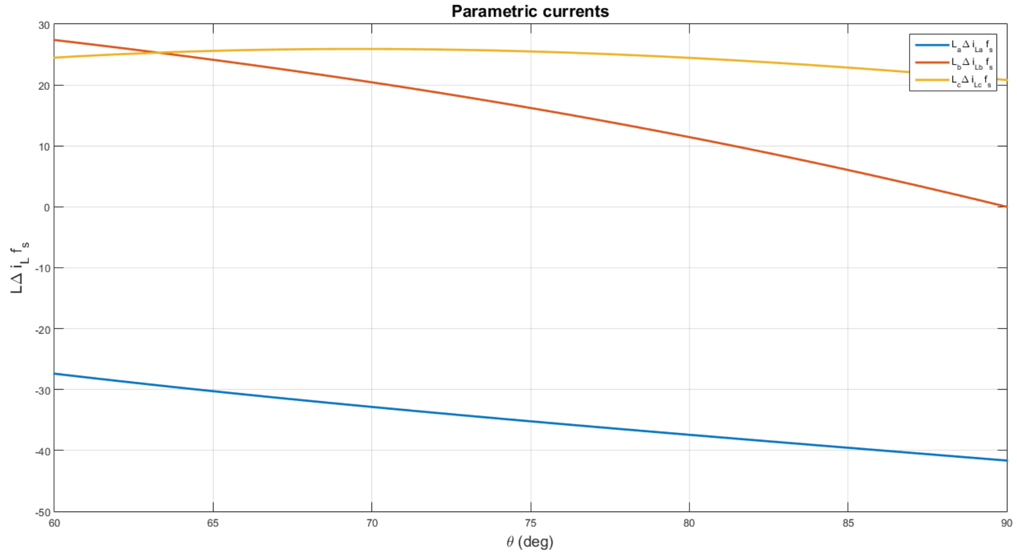

Figure 5.10: Graphical representation of the parametric currents shown in equations 5.4 and 5.5.

to the same current ripple. Therefore, L can be calculated by equation 5.7

$$L = \frac{V_p}{V_i}\frac{(V_i - 1.5V_p)}{\Delta i_{Lmax} f_s} \tag{5.7}$$

Equation 5.7 is used taking the specifications given in table 5.1. The first step is to find the converter output peak current.

$$I_{opk} = \frac{2P}{3\eta V_{opk}} = \frac{2 \times 12000}{3 \times 0.95 \times 120 \times \sqrt{2}} = 49.6\ A \tag{5.8}$$

The maximum current ripple is required to be less than or equal to 4% of that value, that is, $\Delta_i Lmax = 0.04 \times 49.6 = 1.984\ A$. Substituting all the values in equation 5.7 gives the desired value.

$$L = \frac{(\sqrt{2} \times 120)}{500}\frac{(500 - 1.5 \times \sqrt{2} \times 120)}{1.984 \times 20000} = 2.1\ mH \tag{5.9}$$

5.1.2 Input capacitor specification

The input capacitor $\mathrm{C_i}$ is determined using the hold-up time criterion[16], according to which the capacitor must be able maintain its terminal voltage within predetermined levels for a time Δt_{hold} assuming that the grid is down.

The capacitor current is given by

$$i_{ci}(t) = C_i \frac{dv_{ci}(t)}{dt} \tag{5.10}$$

which can be approximated by

$$I_i = C_i \frac{\Delta V_{ciH}}{\Delta t_{hold}} \tag{5.11}$$

where $\mathrm{I_i}$ is the converter nominal input current and $\Delta \mathrm{V_{ciH}}$ is the maximum voltage change acceptable. The nominal input current is calculated according to equation 5.12

$$I_i = \frac{P}{\eta V_i} \tag{5.12}$$

Substituting equation 5.12 into equation 5.11 leads to the following expression, from which the input capacitor can be determined.

$$C_i = \frac{P \Delta t_{hold}}{\eta \Delta V_{ciH} V_i} \tag{5.13}$$

Utilizing the data given in table 5.1 the capacitor can be determined as shown in equation 5.14.

$$C_i = \frac{12000 \times 0.0055}{0.95 \times 0.1 \times 500^2} = 2.8\ mF \tag{5.14}$$

Now that all the important system parameters and components have been specified, the current and voltage compensation systems can be designed.

5.2 Compensation systems design

5.2.1 Current compensation system design

Section 4.1.1 presented the converter model for current control. From equation 4.27

$$\frac{\widetilde{i}_d(s)}{\widetilde{d}'(s)} = G(s) = -\frac{V_i}{sL + R} \tag{5.15}$$

Substituting the values given in table 5.1 into equation 5.15 leads to

$$G(s) = -\frac{500}{0.0021s + 0.57} \tag{5.16}$$

The goal now is to develop a controller that will make the converter output current to track a step reference current with zero error in the steady state. Figure 5.11 shows the closed loop system in which H(s) represents the current controller transfer function.

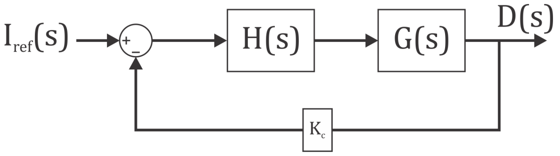

Figure 5.11: Closed-loop system for current control

The Bode plot of G(s) is shown in figure 5.12. Clearly G(s) is unstable as its phase margin is negative. The controller to be designed must guarantee not only closed loop stability but also zero steady-state error. From the last requirement it can be concluded that it must have a pole at the origin. Also, it must advance the open-loop phase in order to increase the phase margin. Equation 5.17 shows the transfer function of a simple controller that can meet both requirements.

$$H(s) = k_i \frac{s + Z_i}{s(s + P_i)} = k_i \frac{s + 2\pi f_z}{s(s + 2\pi f_p)} \tag{5.17}$$

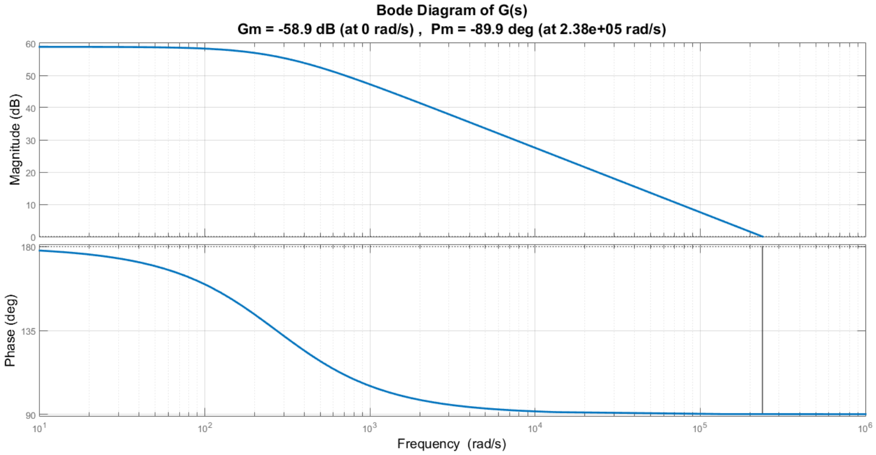

Figure 5.12: Bode plot of G(s)

The 0 dB crossing frequency will be set as one fourth of the sampling frequency, that is, $f_c = \frac{f_s}{4}$. One of the poles is at the origin, the other one will be placed at $f_p = 10 f_c$ in order to minimize the effects of high-frequency switching. The zero will be placed at $f_z = \frac{f_c}{10}$ in order to improve the system phase margin. Also, the gain $\mathrm{k_i}$ must be chosen such that the open-loop gain at the crossover frequency is 1, which leads to

$$k_i = \frac{1}{H(2\pi f_c)G(2\pi f_c)} = -4.1810 \times 10^5 \tag{5.18}$$

Substituting all the values specified above into equation 5.17 results in the transfer function shown in equation 5.19

$$H(s) = -4.1810 \times 10^5 \frac{s + 3142}{s(s + 3.142 \times 10^5)} \tag{5.19}$$

Figure 5.13 shows the Bode plot of the open-loop transfer function $G(s)H(s)k_i$. It can be seen that the phase margin has increased to 79°. The gain margin is infinite, meaning that the system is stable regardless of the gain applied.

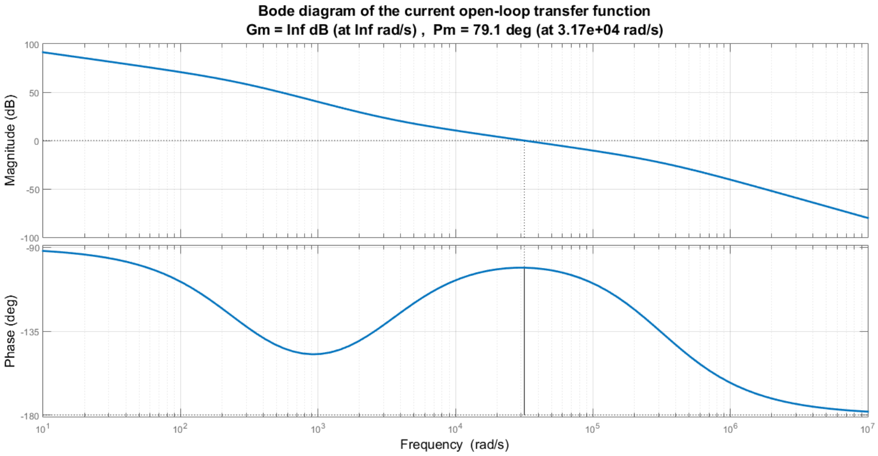

Figure 5.13: Bode plot of the open-loop transfer function

5.2.2 Voltage compensation system design

The next step is to design the voltage compensation system. Figure 5.14 shows the closed-loop system with the inner current loop and the outer voltage loop, where C(s) is the voltage controller to be designed in this section. The voltage and current controllers are designed independently from each other. That can be done only if the inner loop has a much faster dynamics than the outer loop.

In section 4.1.2 the converter model for voltage control was developed. Substi-

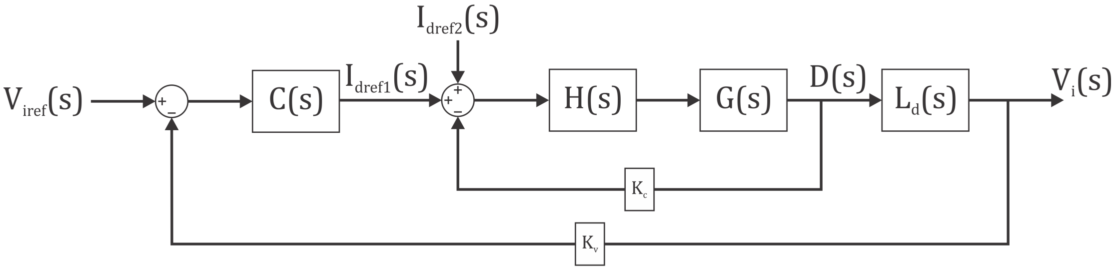

Figure 5.14: Closed-loop system with current and voltage compensators.

tuting the values from table 5.1 into equation 4.55 results in

$$\begin{aligned}
L_d(s) &= \frac{\widetilde{v}_i(s)}{\widetilde{i}_d(s)} = -\frac{1}{V_i}\frac{1}{sC_i}\left[\sqrt{\frac{2}{3}}\frac{L\overline{P}}{V_{ph}}s - \sqrt{\frac{2}{3}}\frac{2R\overline{P}}{V_{ph}} + \sqrt{\frac{3}{2}}V_{ph}\right] \\
L_d(s) &= \frac{-2.425\times 10^{-4}s + 0.2841}{2.8\times 10^{-3}s} \\
L_q(s) &= \frac{\widetilde{v}_i(s)}{\widetilde{i}_q(s)} = -\sqrt{\frac{2}{3}}\frac{\overline{Q}}{V_iV_{ph}}\frac{1}{sC_i}\left[Ls + 2R\right] \\
L_q(s) &= \frac{-2.425\times 10^{-4}s - 0.1316}{2.8\times 10^{-3}s}
\end{aligned} \tag{5.20}$$

The bode plot of $\mathrm{L_d}(s)$ is presented in figure 5.15. The system has a gain margin of -21.25 dB and a phase margin of -95.2º, showing that the system is unstable.

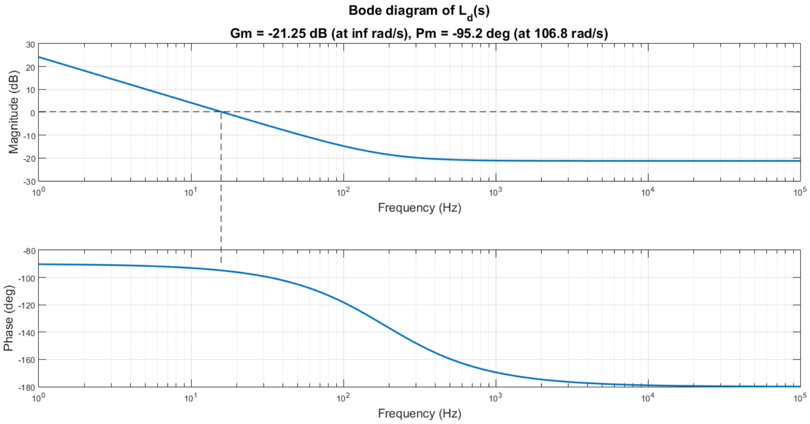

Figure 5.15: Bode plot of $L_d(s)$.

A PI controller is going to be used in order to stabilize the system. The controller transfer function is shown in equation 5.21

$$C(s) = k_{pi} \frac{s + Z_v}{s} \tag{5.21}$$

The crossover frequency of the voltage loop must be much smaller than the crossover frequency of the current loop in order guarantee that the two loops are decoupled. The voltage loop crossover frequency will be set as one third of the grid frequency.

$$f_{cv} = \frac{f_g}{3} = \frac{60}{3} = 20\ Hz \tag{5.22}$$

The controller zero will be placed at

$$f_{zv} = \frac{f_g}{12} = \frac{60}{12} = 5\ Hz \tag{5.23}$$

The gain $\mathrm{k_{pi}}$ must be chosen such that the open-loop gain at the crossover frequency is 1

$$k_{pi} = \frac{1}{L_d(2\pi f_c) C(2\pi f_c) K_v} = 111 \tag{5.24}$$

Substituting all the values specified in the previous equations into equation 5.21 results in the transfer function shown in equation 5.25

$$C(s) = \frac{111S + 3487}{s} \tag{5.25}$$

Figure 5.16 shows the voltage open-loop bode diagram. It can be seen that the gain and phase margins have been significantly improved.

This chapter presented the system specifications and the design of the current and voltage compensation systems. Next chapter will present and discuss the simulation

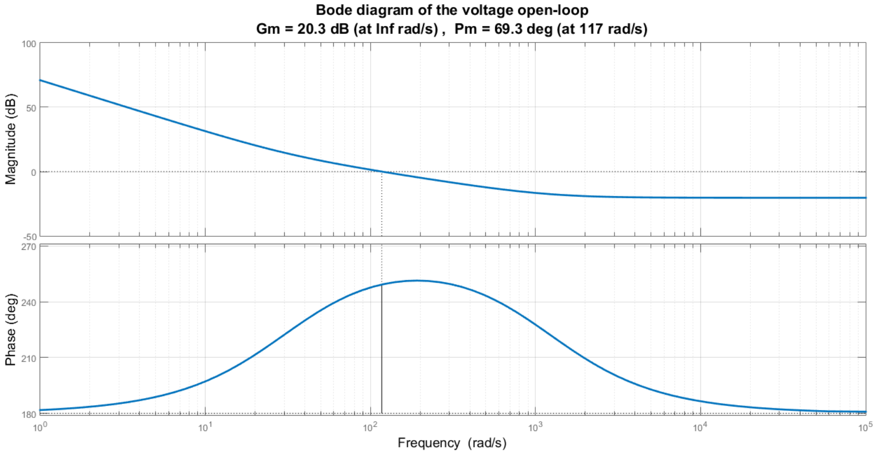

Figure 5.16: Duty cycle over section 2.

results.

6. SIMULATIONS

Chapter 5 discussed the converter and control system design. The values found there will be used to simulate the system and the results will be shown in this chapter. For convenience, the most important parameters presented in chapter 5 are summarized below.

Table 6.1: System specifications

P = 12 kVA
$\mathrm{V_{out}}$ = 120 V
f_g = 60 Hz
f_s = 20 kHz
$\mathrm{K_c}$ = 0.1
$\mathrm{K_v}$ = 0.01
$\mathrm{C_i}$ = 2.8 mF
L = 2.1 mH
R = 0.575 Ω

$$G(s) = -\frac{500}{0.0021s + 0.57} \tag{6.1}$$

$$H(s) = -4.1810 \times 10^5 \frac{s + 3142}{s(s + 3.142 \times 10^5)} \tag{6.2}$$

$$L_d(s) = \frac{-2.425 \times 10^{-4}s + 0.2841}{2.8 \times 10^{-3}s} \tag{6.3}$$

$$C(s) = \frac{111S + 3487}{s} \tag{6.4}$$

6.1 System Simulink® model

Figure 6.1 shows the Simulink® model for the power circuit. From the figure it can be seen that the model is composed of a three-phase voltage source representing the grid, a PV array model got from the Simulink® library, the PWM active filter converter, a transformer, a three-phase rectifier and a three-phase inductive load. The last two items were chosen to represent the linear and non-linear loads that are usually connected to the grid. The converter is supposed to extract the maximum power from the solar array whenever there is power to be extracted. In addition, it is supposed to always perform harmonic compensation.

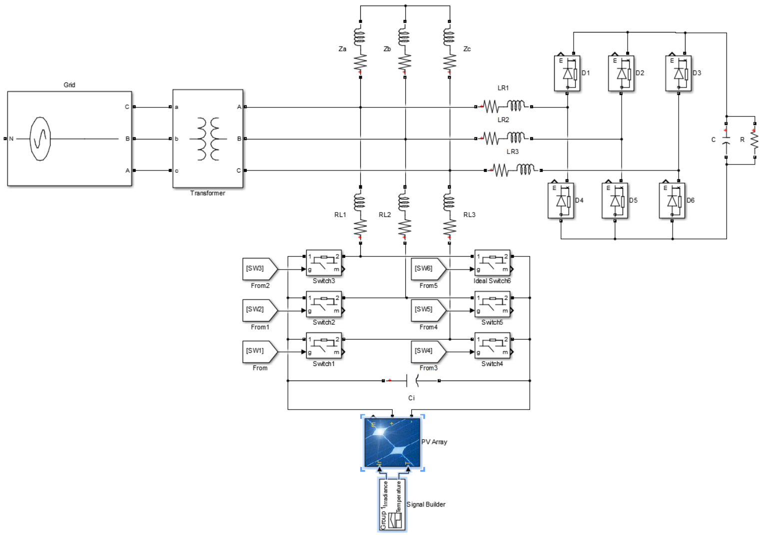

Figure 6.1: Simulink® model of the power circuit.

Figures 6.2-6.7 show the different parts of the control system. Figure 6.2 shows the system section in which the phase currents from the load and the converter are converted into line currents.

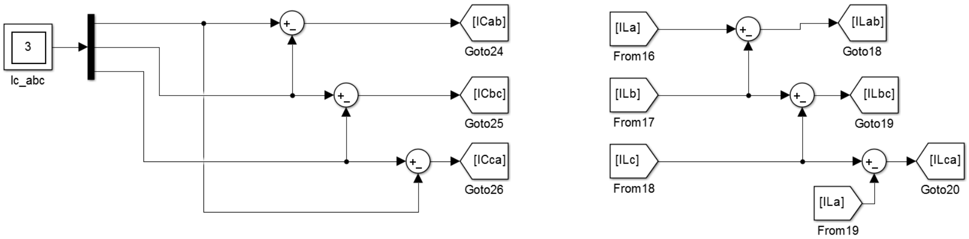

Figure 6.2: Transformation of the phase current into line currents.

Then, the line currents are transformed into the dq0 domain, as shown in figure 6.3

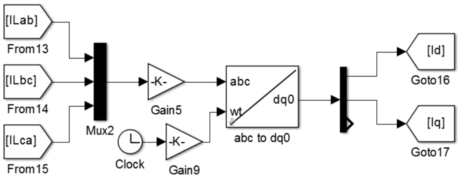

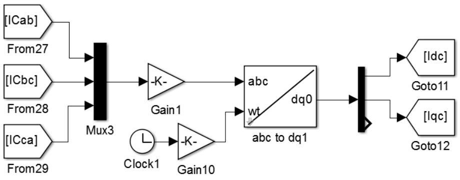

Figure 6.3: Transformation of ABC line currents into dq0 currents.

The P&O block shown in figure 6.4 implements the perturb and observe MPPT algorithm. The output voltage and current of the PV array are measured and used as inputs to the block. The P&O output signal is then combined with a constant voltage signal to compose the voltage reference signal, as explained in subsection 4.1.2. The reference signal is compared to the measured voltage and the error signal

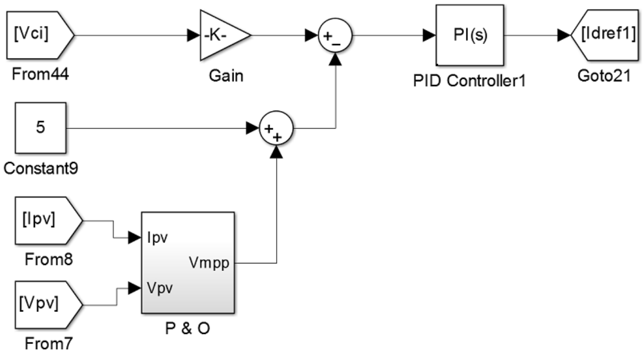

Figure 6.4: Voltage control loop.

is applied to the voltage controller. The controller output signal is then used as a reference signal by the current controller.

Figure 6.5 shows the two control loops used to control the d and q-axis currents. The signal coming out of the voltage controller and the filtered d-axis load current are used as references by the d-axis current controller. The q-axis current controller use the unfiltered q-axis load current as a reference to the converter current. In that way the controllers make sure that the converter will generate the necessary harmonic current at the same time it keeps the capacitor voltage constant.

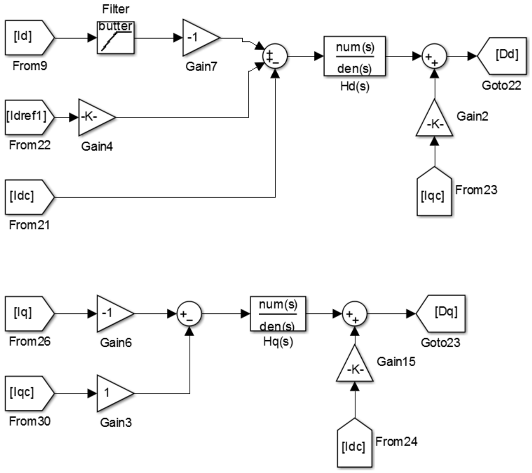

Figure 6.5: Current control loop.

The current compensation system generate the phase-to-phase dq0 duty cycles necessary to perform PWM modulation. Before being used, those signals must be transformed twice, one from the dq0 domain into the ABC domain, and other from phase-to-phase to phase. Figure 6.6 shows the circuit sections responsible for those conversions.

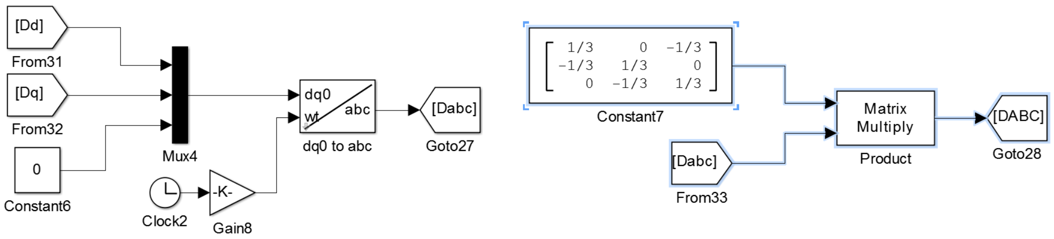

Figure 6.6: Duty cycle conversion from dq0⟶ABC and phase-to-phase⟶phase.

Last, the duty cycles signals are used in the PWM modulation circuit, as shown in figure 6.7.

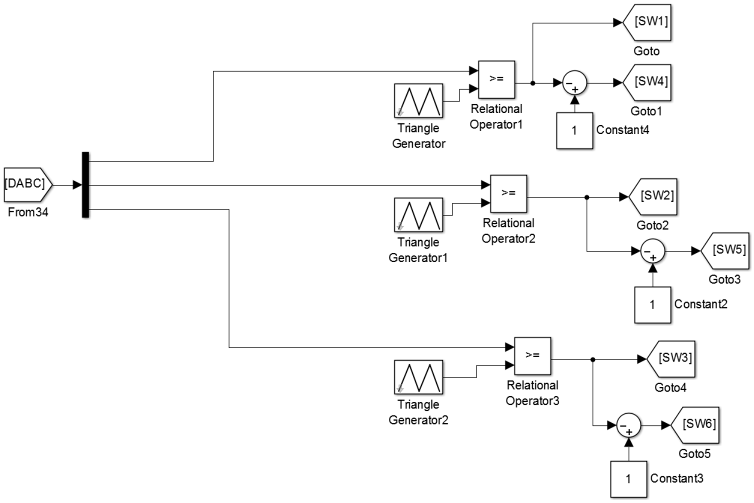

Figure 6.7: PWM modulation section.

6.2 Waveforms

In order to demonstrate its functionality, the system will be simulated under different temperature and irradiation conditions. Figure 6.8 shows the array IV and PV curves for two different temperatures, T = 25°C and T = 40°C, under constant irradiance. It can be seen that $V_{mp} = 499.7$ V for T = 25°C and $V_{mp} = 466.4$ V for T = 40°C.

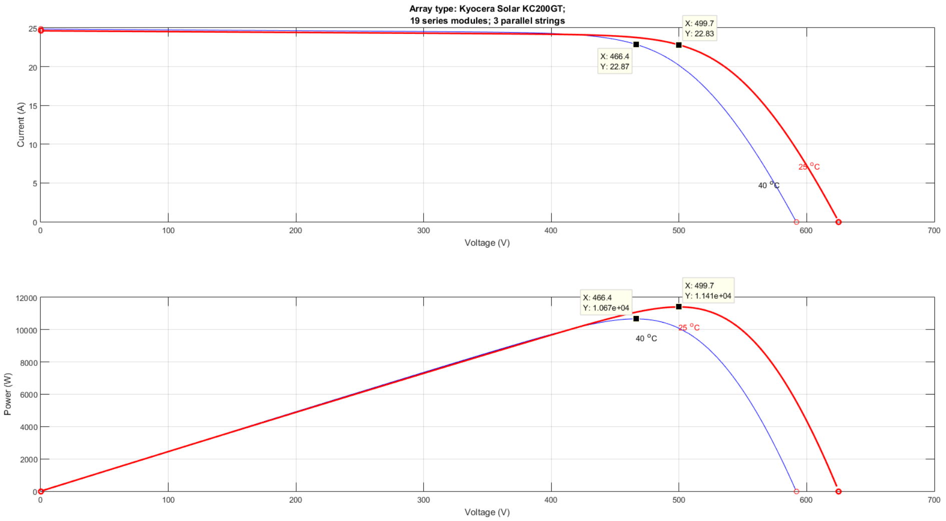

Figure 6.8: IV and PV curves for different different temperatures and I = 1000 W/m^2.

- T = 25°C and I = 0

In the first simulation T = 25°C and I = 0. Those values correspond to the night time condition, when there is no sunlight reaching the array and the temperature is mild. In that case the converter is working simply as an active filter performing harmonic compensation. Figure 6.9 shows the capacitor voltage. Since the PV array is not generating any power, the P&O block output is zero, making the reference voltage constant and equal to 500 V.

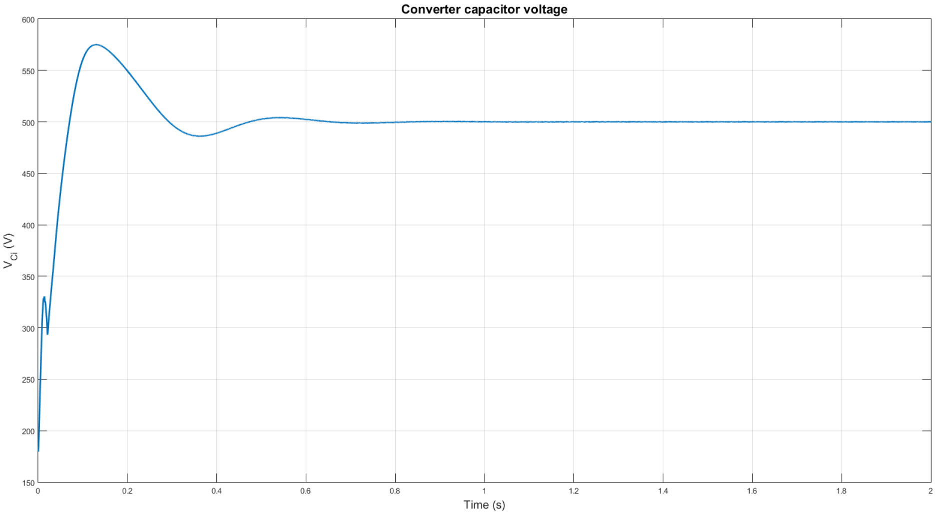

Figure 6.9: Capacitor voltage - T = 25°C, I = 0 W/m^2.

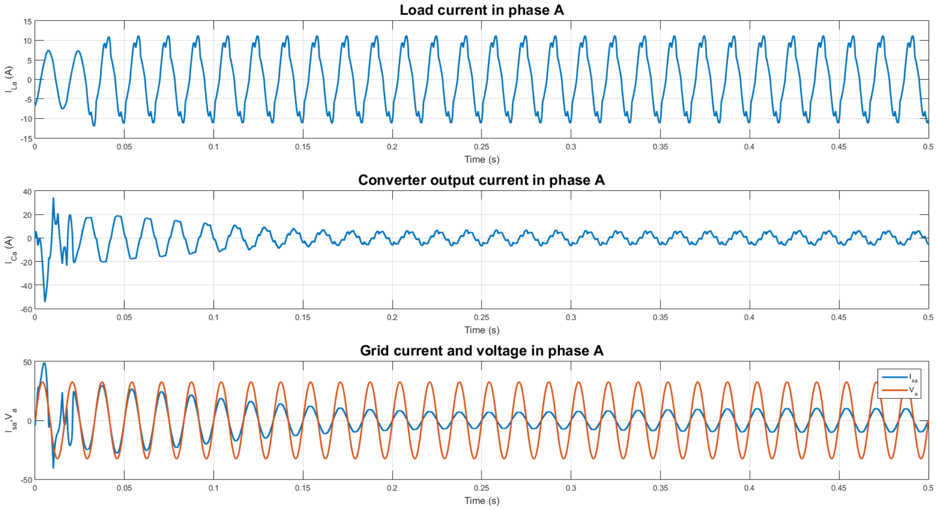

Figure 6.10: Load, converter and grid currents in phase A when T = 25°C and I = 0 W/m^2.

Figure 6.10 shows the load current, the converter output current and the current flowing out of the grid. It can be seen that although the load current is highly distorted, the grid current is very close to a sinusoid. That is due to the harmonic compensation performed by the converter that monitors the harmonic current being drawn by the load and generates its harmonic content. Since the load current is the sum of the converter plus the grid current and the converter is already generating all the current harmonic content, the grid has to provide only the fundamental harmonic of the load current. Figure 6.11 shows the waveforms in greater detail. A rescaled version of phase A grid voltage is plotted along with the load and the grid current. It is clear that the converter not only compensate the high frequency harmonics, but also shifts the current in such a way that it stays in phase with the voltage.

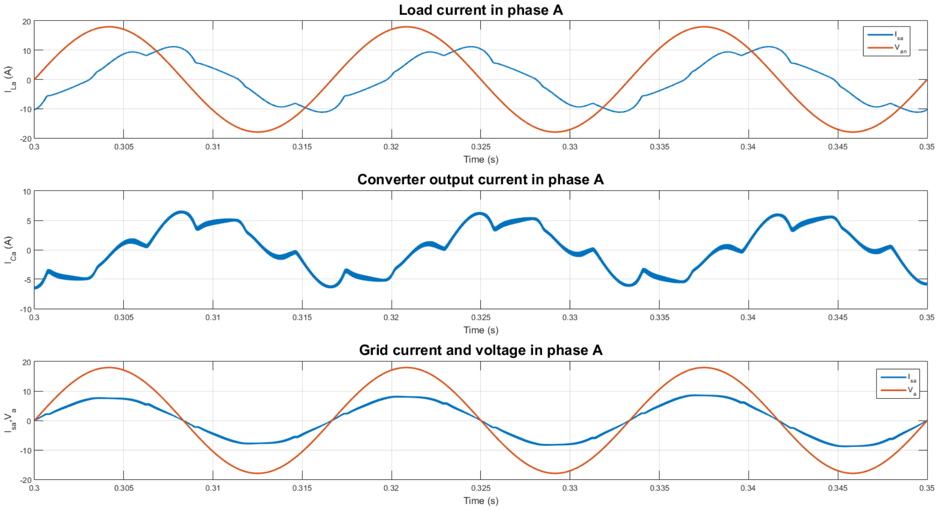

Figure 6.11: Rescaled version of figure 6.10.

- T = 40ºC and I = 1000 W/m^2

Next, the system is simulated for T = 40ºC and I = 1000 W/m^2. That corresponds to a day time condition with good irradiance reaching the array and increasing its temperature. From figure 6.8 it is seen that the maximum power point voltage is 466 V for the conditions simulated here. Figure 6.12 shows that after a transient period, the capacitor voltage reaches the value expected, which shows the efficacy of the MPPT algorithm.

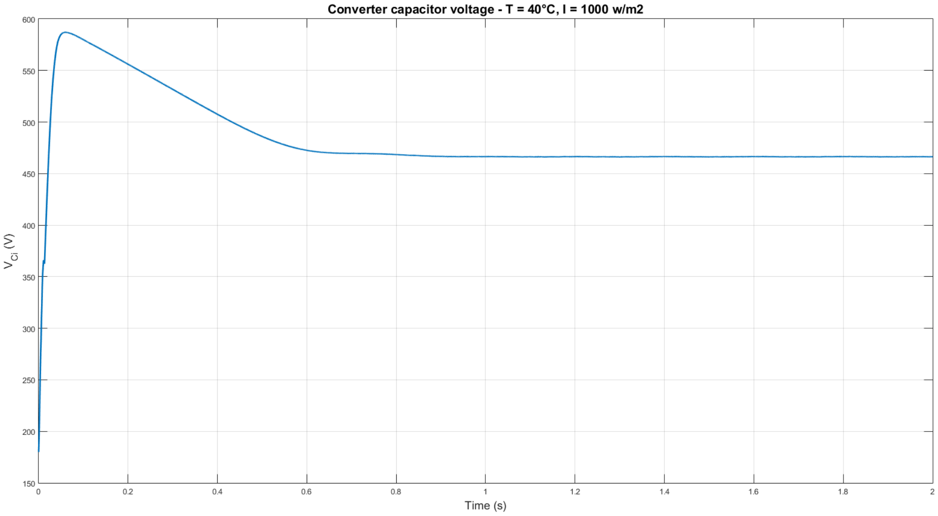

Figure 6.12: Capacitor voltage - T = 40°C, I = 1000 W/m^2.

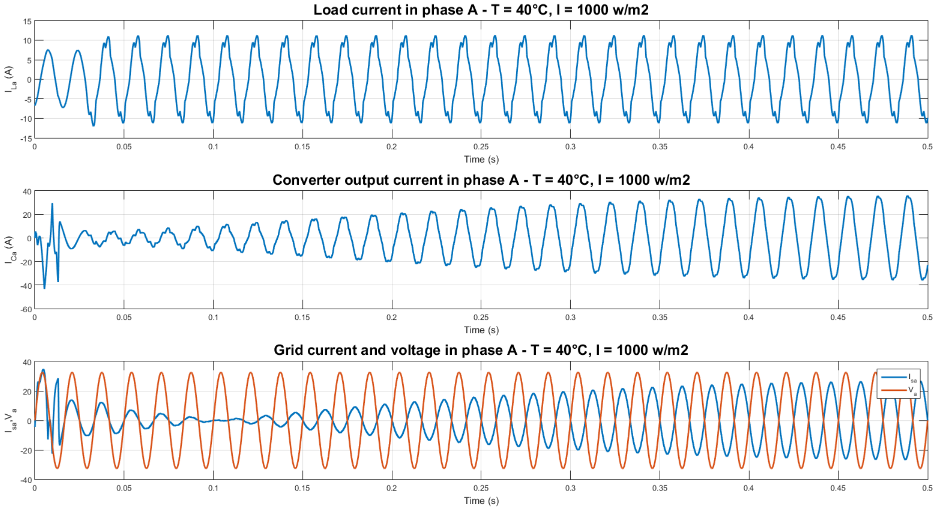

Figure 6.13: Load, converter and grid currents in phase A when T = 40°C and I = 1000 W/m^2.

The load, converter and grid currents are shown in figures 6.13 and 6.14. From these figures it can be seen that the grid current and the grid voltage are 180° phase shifted from each other. That means active power is flowing into the grid, which happens when the power generated by the PV array is higher than the power demanded by the load.

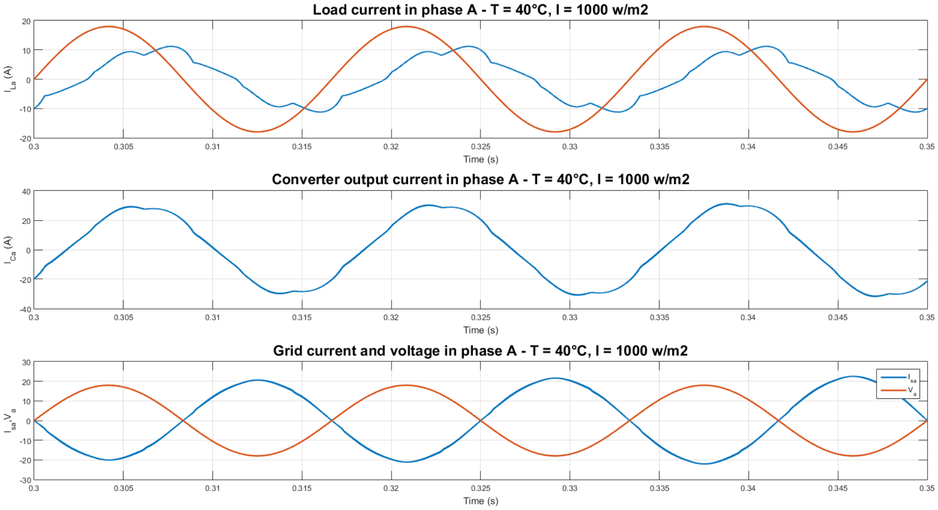

Figure 6.14: Rescaled version of figure 6.13.

- T = 25°C - 40°C and I = 0 W/m^2-1000 W/m^2

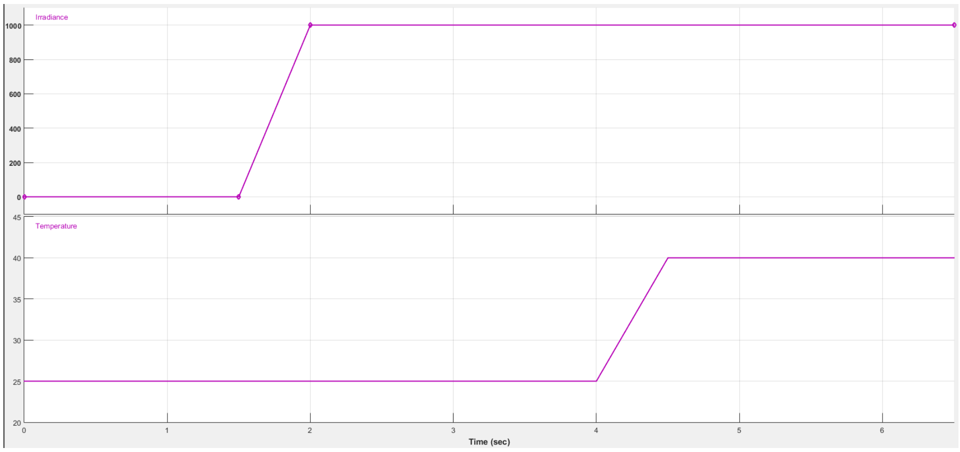

Figure 6.15: Irradiance and temperature signals.

In the next simulation both irradiance and temperature vary according to figure 6.15. From t = 0 s to t = 1.5 s, T = 25°C and I = 0 W/m^2, which corresponds the night time condition discussed before. Then, at t = 1.5 s the irradiance begins to increase and reaches I = 1000 W/m^2 at t = 2.0 s. At t = 4 s the temperature also begins to increase and reaches 40 °C 0.5 second later.

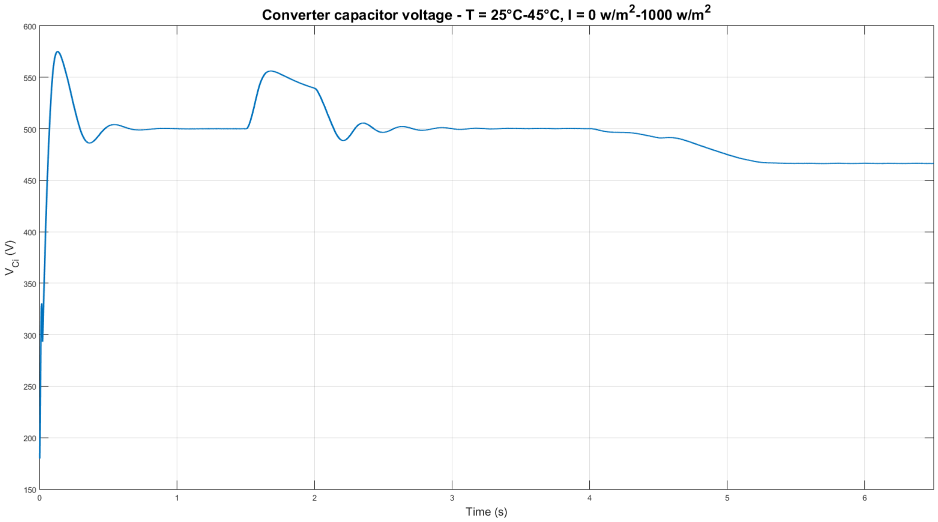

Figure 6.16: Capacitor voltage for the varying temperature and irradiance shown in figure 6.15.

Figure 6.16 shows the capacitor voltage during that time interval. In the first section (from t = 0 s to t = 1.5 s) the PV array does not generate power, the MPPT block output is zero and the reference voltage is constant and equal to 500 V. In the second section (from t = 2 s to t = 4 s), T = 40 °C and I = 1000 W/m^2. Under that condition figure 6.8 shows that V_{mp} = 499.6 V. From figure 6.16 it can be seen that after a short transient beginning at t = 1.5 s, V_{Ci} reaches V_{mp}. In the last section (from t = 4.5 s to t = 6.5 s), T = 40 °C and I = 1000 W/m^2. From figure 6.8 V_{mp} = 466.4 V. That is the value that V_{Ci} converges to after a transient beginning at t = 4 s.

Figures 6.17 and 6.18 show the current waveforms. It can be seen that in the first section, from t = 0 to around t = 1.65 s, the PV panel is not generating power.

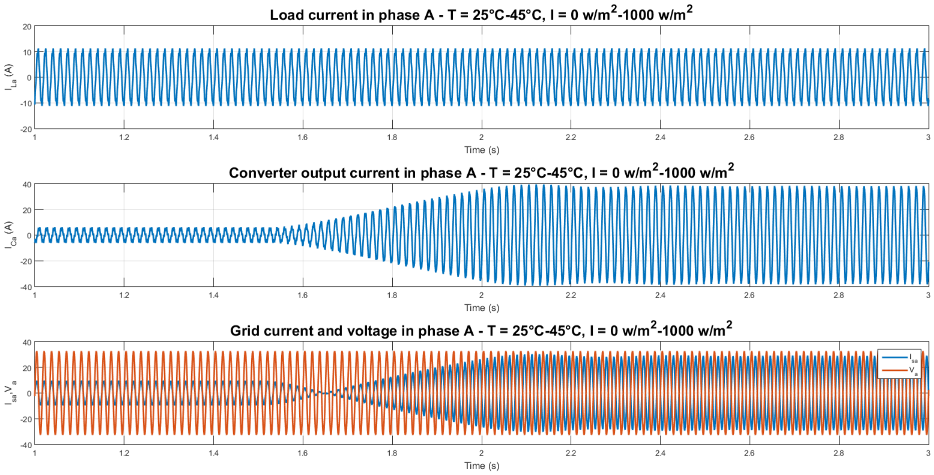

Figure 6.17: Load, converter and grid currents in phase A when T and I vary according figure 6.15.

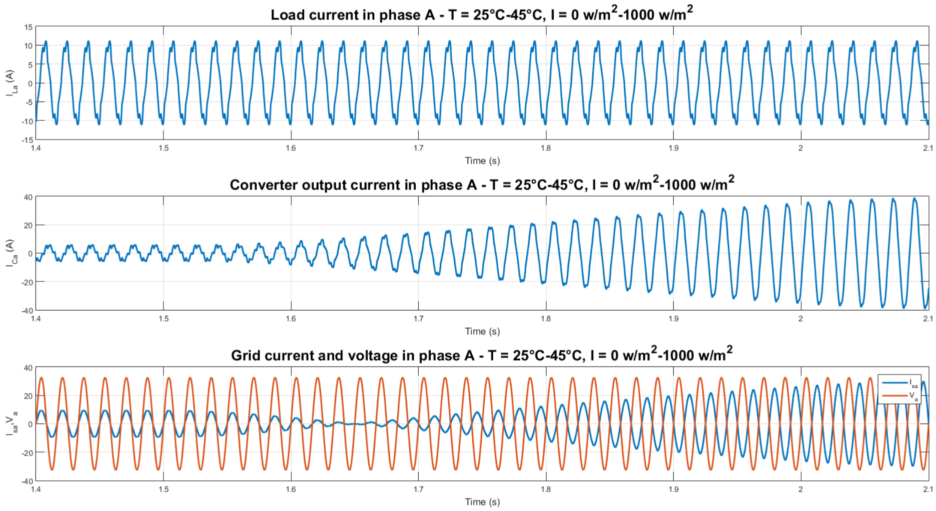

Figure 6.18: Rescaled version of figure 6.17.

The converter current is small, corresponding to the harmonic current drawn by the load. The grid current is in phase with the grid voltage, meaning that power is being drawn from the grid. When the irradiance becomes greater than zero, which occurs at t = 1.5 s, the PV array begins to produce power. The grid current decreases and eventually changes its direction (around t = 1.65 s). From that moment on the power flows from the PV panel to the load and grid.

- Non-linear load at T = 25°C and I = 0 W/m^2

In the last simulation the load is assumed to be exclusively non-linear. The three-phase linear load shown in figure 6.1 is removed leaving only the three-phase rectifier connected to the grid. The irradiance is reduced to 0 W/m^2 and temperature is kept at 25 °C. Figure 6.19 shows the capacitor voltage. As expected, after a transient of around 0.6 s, the voltage reaches a steady state value of approximately 499.9 V, which corresponds the voltage previously established for the no-light situation.

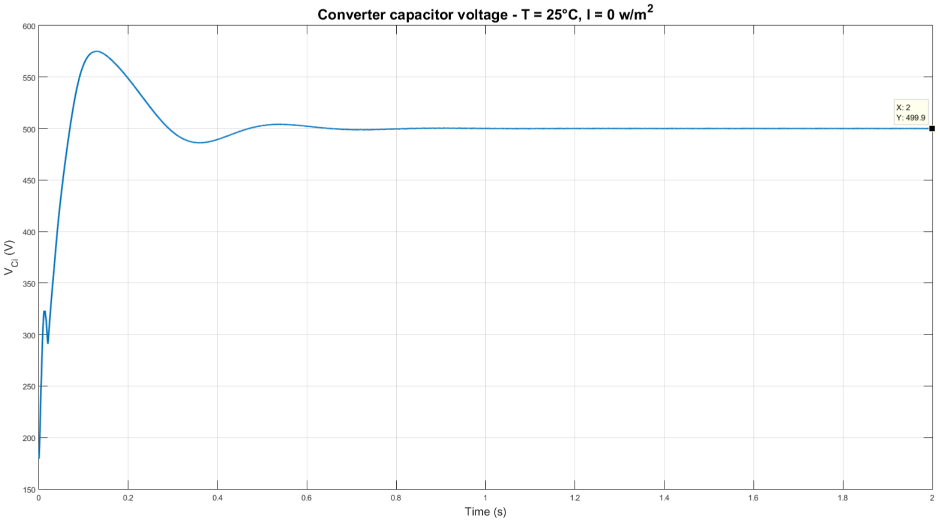

Figure 6.19: Capacitor voltage - T = 25°C, I = 0 W/m^2.

Figure 6.20 shows the current waveforms. It can be seen that the load current is considerably distorted. Figure 6.21 shows that besides the fundamental, I_{LA} has all the odd harmonics but the multiples of the third one. On the other hand, the current drawn from the grid is almost a pure sinusoidal. The spectral analysis of I_{SA} illustrated in figure 6.22 shows that the its harmonic content is almost zero.

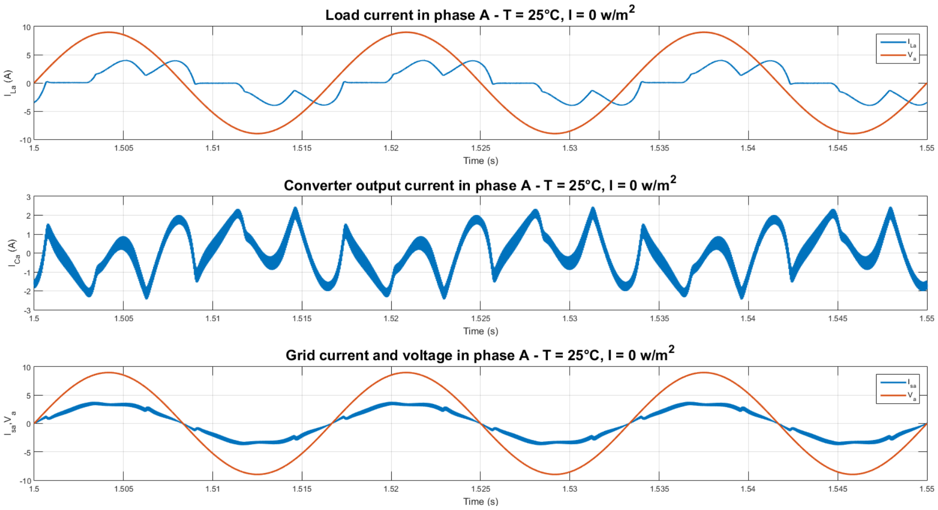

Figure 6.20: Load, converter and grid currents in phase A when T = 25°C and I = 0 W/m^2.

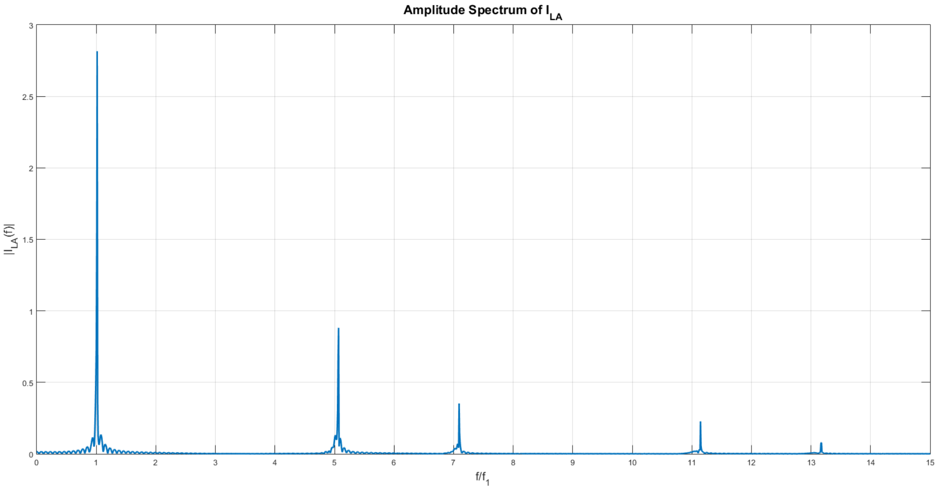

Figure 6.21: Frequency spectrum of I_{LA} obtained through FFT analysis

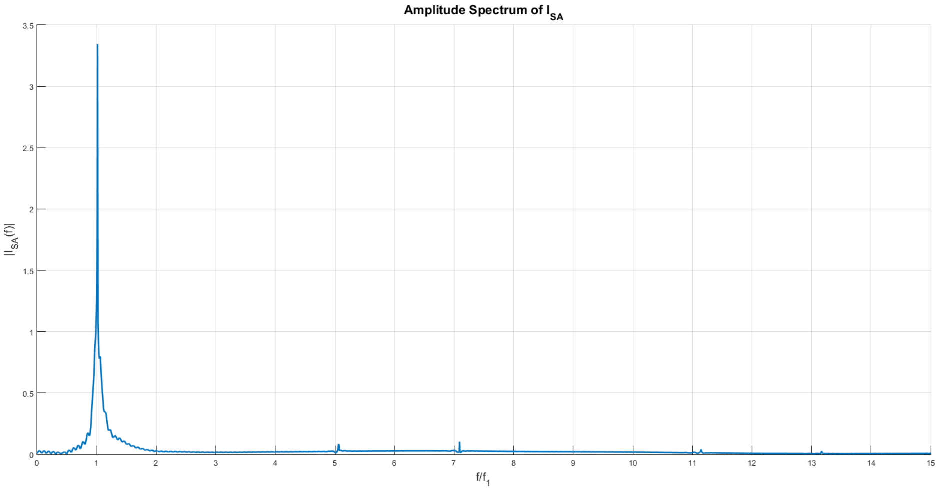

Figure 6.22: Frequency spectrum of I_{SA} obtained through FFT analysis

7. CONCLUSION

This thesis presented and discussed a three-phase converter capable of performing harmonic compensation and maximum power point tracking in a grid-connected PV panel application. The converter is essentially a shunt active filter, traditionally used to do harmonic compensation, which was modeled and controlled to simultaneously perform maximum power point tracking of a PV array connected across the filter capacitor.

Chapter 1 provided the context in which such technology may be utilized. With the growing importance of renewable energy sources in face of the global warming and the foreseen exhaustion of non-renewable sources, PV panels are expected to be widely employed in stand-alone and grid-connected applications. In that scenario the system described in this thesis could be used with great advantage for the user.

Chapter 2 explained the mathematical basis used to control the converter. The chapter discussed the classical and the instantaneous power theories, contrasted them with each other and showed why the former must be used in the implementation of a real time harmonic compensator like the active filter.

Chapter 3 focused on the fundamentals of solar energy. It gave basic information about the behavior of solar cells resorting to elementary quantum physics. Based on that, it showed how a circuit model can be developed to explain the terminal characteristics of a PV panel. The understanding of PV panel terminal characteristics is crucial to extract the maximum power from it. The chapter also explained a few maximum power point tracking algorithm, two of which were used in the system considered in this thesis.

Chapter 4 presented the modeling of the PWM circuit. The model was important to develop the control system necessary to make the converter to behave in the expected way.

Chapter 5 detailed the control system design, which was based on the model developed in chapter 4. It also showed how to design some of the power circuit components.

Finally, chapter 6 presented the simulation results. It was shown that the converter behaves as expected, performing harmonic compensation and tracking the maximum power point for different temperature and irradiance conditions.

The work presented here gives rise to interesting questions whose answers will be pursued in the future. One question is how the system behaves under unbalanced load conditions. That is a common situation in residential applications, where most of the loads are single-phase, and it can happen even in a three-phase system if the load is defective.

Another question is how the MPPT algorithm dynamics influences the whole system behavior. It is clear that the MPPT tracking algorithm must be much slower than the converter (in the circuit modeling the capacitor voltage was assumed to be constant). But how much slower must it be? The answer to this question, as well as to the previous one, will be searched next.

REFERENCES

[1] U.S. Energy Information Administration. Primary energy overview, 2016.

[2] Hirofumi Akagi, Yoshihira Kanazawa, Koetsu Fujita, and Akira Nabae. Generalized theory of instantaneous reactive power and its application. *Electrical engineering in Japan*, 103(4):58–66, 1983.

[3] Hirofumi Akagi, Edson Hirokazu Watanabe, and Mauricio Aredes. *Instantaneous power theory and applications to power conditioning*, volume 31. John Wiley & Sons, 2007.

[4] Paul A Basore, Donald Chung, and Tonio Buonassisi. Economics of future growth in photovoltaics manufacturing. In *Photovoltaic Specialist Conference (PVSC), 2015 IEEE 42nd*, pages 1–4. IEEE, 2015.

[5] D. Borgonovo, Y. R. de Novaes, and I. Barbi. A three-phase three-switch two-level pwm rectifier. In *Power Electronics Specialist Conference, 2003. PESC '03. 2003 IEEE 34th Annual*, volume 3, pages 1075–1079 vol.3, June 2003.

[6] Deivis Borgonovo. Modelagem e controle de retificadores pwm trifásicos empregando a transformação de park. florianópolis, 2001. Master's thesis, Dissertação de Mestrado em Engenharia Elétrica–INEP, UFSC., 2001.

[7] Richard Burrett, Corrado Clini, Robert Dixon, Michael Eckhart, Mohamed El-Ashry, Deepak Gupta, Amal Haddouche, David Hales, Kirsty Hamilton, UK Chatham House, et al. Renewable energy policy network for the 21st century. 2015.

[8] John Cook, Dana Nuccitelli, Sarah A Green, Mark Richardson, Bärbel Winkler, Rob Painting, Robert Way, Peter Jacobs, and Andrew Skuce. Quantifying the

consensus on anthropogenic global warming in the scientific literature. *Environmental Research Letters*, 8(2):024024, 2013.

[9] M. A. G. de Brito, L. Galotto, L. P. Sampaio, G. d. A. e Melo, and C. A. Canesin. Evaluation of the main mppt techniques for photovoltaic applications. *IEEE Transactions on Industrial Electronics*, 60(3):1156–1167, March 2013.

[10] Renewable Energy Policy Network for the 21st Century(REN21). Renewables 2015 global status report. Technical report, 2015.

[11] Heinrich Häberlin. *Photovoltaics system design and practice.* John Wiley & Sons, 2012.

[12] Richard Heinberg. Searching for a miracle. In *Net Energy Limits & the Fate of Industrial Society. A Study for the International Forum on Globalization. San Francisco*, 2009.

[13] C Kittel. Introduction to solid state physics, 6th edn., translated by y. *Uno, N. Tsuya, A. Morita and J. Yamashita,(Maruzen, Tokyo, 1986) pp*, pages 124–129, 1986.

[14] Kyocera. Instalation manual for the kc125gt kc200gt. Technical note.

[15] Roger Messenger and Amir Abtahi. *Photovoltaic systems engineering.* CRC press, 2010.

[16] ST Microelectronics. Power supply hold-up time, 2007. Technical note.

[17] J.W. Nilsson and S.A. Riedel. *Electric Circuits.* Always learning. Pearson Education, 2015.

[18] United Nations Department of Economics and Social Affairs. 2015 revision of world population prospects, March 2016.

[19] R.K. Pachauri and L.A. Meyer. Climate change 2014: synthesis report. summary for policymakers. In *Climate change 2014: synthesis report. Summary for policymakers*. IPCC, 2014.

[20] M. F. Schonardie, R. F. Coelho, R. Schweitzer, and D. C. Martins. Control of the active and reactive power using dq0 transformation in a three-phase grid-connected pv system. In *Industrial Electronics (ISIE), 2012 IEEE International Symposium on*, pages 264–269, May 2012.

[21] Shahriar Shafiee and Erkan Topal. When will fossil fuel reserves be diminished? *Energy Policy*, 37(1):181 – 189, 2009.